Aerosol mass and optical properties, smoke influence on O3, and high NO3 production rates in a western US city impacted by wildfires

Vanessa Selimovic[1], Robert J. Yokelson[1], Gavin Robert McMeeking[2], and Sarah Coefield[3]

[1]University of Montana
[2]Handix Scientific
[3]Missoula City-County Health Department

November 23, 2022

Abstract

Evaluating our understanding of smoke from wild and prescribed fires can benefit from downwind measurements that include both inert tracers to test production and transport and reactive species to test chemical mechanisms. We characterized smoke from fires in coniferous forest fuels for >1000 hours over two summers (2017 and 2018) at our Montana surface station and found a narrow range of key properties. DPM/DCO was 0.1070 +/- 0.0278 or about half the age-independent ratios obtained at free troposphere elevations. The average absorption Angstrom exponent across both years was 1.84, or about half the values available for very fresh smoke. Brown carbon (BrC) was persistent (~50% of the absorption at 401 nm) in both years, despite differences in smoke age and transport. DBC/DCO doubled from 2017 to 2018, but the average across two years was within 30% of recent airborne measurements. Switching from a 1.0 to a 2.5 micron cutoff increased the mass scattering and mass absorption coefficients suggesting super micron particles impact the optical properties of moderately aged smoke. O3 was elevated ~6 ppb on average over a full diurnal period when wildfire smoke was present, and smoke-associated O3 increases were highest (~9 pbb) at night suggesting substantial upwind production. NOx was almost entirely local in origin. NO2 spurred high rates of NO3 production in the presence of wildfire smoke (up to 2.44 ppb/hr) and potentially at least one nighttime BrC formation event that could have impacted next-day photochemistry.

Aerosol mass and optical properties, smoke influence on O_3, and high NO_3 production rates in a western US city impacted by wildfires

Vanessa Selimovic[1], Robert. J. Yokelson[1], Gavin R. McMeeking[2], and Sarah Coefield[3]

[1]Department of Chemistry, University of Montana, Missoula, 59812, USA
[2]Handix Scientific LLC, 5485 Conestoga Court, Suite 104B, Boulder, CO, 80301, USA
[3]Missoula City-County Health Department, Missoula, MT, 59801, USA

Corresponding author: Robert. J. Yokelson (bob.yokelson@umontana.edu)

Key Points:

- We measured tracers and reactive species in smoke for more than 1000 hours at a western US surface site downwind of many wildfires.
- The ratio of both particulate matter and brown carbon to carbon monoxide was consistently about half the usual ratio in fresh smoke.
- Ozone was enhanced by more than 10 percent during smoke episodes in a diurnal pattern suggesting significant regional enhancement.

Abstract

Evaluating our understanding of smoke from wild and prescribed fires can benefit from downwind measurements that include both inert tracers to test production and transport and reactive species to test chemical mechanisms. We characterized smoke from fires in coniferous forest fuels for >1000 hours over two summers (2017 and 2018) at our Montana surface station and found a narrow range of key properties. $\Delta PM_{2.5}/\Delta CO$ was 0.1070 ± 0.0278 or about half the age-independent ratios obtained at free troposphere elevations. The average absorption Ångström exponent across both years was 1.84, or about half the values available for very fresh smoke. Brown carbon (BrC) was persistent (~50% of the absorption at 401 nm) in both years, despite differences in smoke age and transport. $\Delta BC/\Delta CO$ doubled from 2017 to 2018, but the average across two years was within 30% of recent airborne measurements. Switching from a 1.0 to a 2.5 micron cutoff increased the mass scattering and mass absorption coefficients suggesting super micron particles impact the optical properties of moderately aged smoke. O_3 was elevated ~6 ppb on average over a full diurnal period when wildfire smoke was present, and smoke-associated O_3 increases were highest (~9 pbb) at night suggesting substantial upwind production. NO_x was almost entirely local in origin. NO_x spurred high rates of NO_3 production in the presence of wildfire smoke (up to 2.44 ppb hr^{-1}) and potentially at least one nighttime BrC formation event that could have impacted next-day photochemistry.

Plain Language Summary

Wildfires are complicated and difficult to sample. We characterized smoke for over 1000 hours downwind of a large number of wildfires burning at all stages and measured species sensitive to total smoke production, the combustion characteristics, and plume evolution. The PM/CO ratio was about half that in fresh smoke suggesting that aerosol evaporation dominates at the surface

at smoke ages up to ~1-2 days. Brown carbon accounted for about half of aerosol absorption at 401 nm. O_3 levels increased significantly during smoke episodes. High NO_3 production rates were driven by local (non-fire) NO_2 sources.

1 Introduction

Biomass burning (BB) is a major source of trace gases and particulate matter (PM) that can significantly impact local, regional, and global atmospheric chemistry; air quality; climate forcing; visibility; and human health (Crutzen and Andreae, 1990; United States Environmental Protection Agency, 2016). BB is one of the largest global sources of fine organic aerosol (OA), black carbon (BC), brown carbon (BrC) (Bond et al., 2004; 2013; Akagi et al., 2011; Hecobian et al., 2010), greenhouse gases, and non-methane organic gases (NMOG) (Yokelson et al., 2008; 2009), which are precursors for the formation of ozone (O_3) and OA. Regionally, in the western US, wildfires produce almost twice as much $PM_{1.0}$ (particles with diameter $\leq$ 1.0 μm) per year as all other western aerosol sources combined (Liu et al., 2017), and frequently have large air quality impacts on extensive regions of the western US, including urban areas.

Wildfires are a key component of forest ecosystems with naturally occurring average frequency in the absence of human influences. However, climate change, the build-up of fuels due to fire suppression, and the expansion of the wildland-urban interface (WUI) have led to increased fire risk and fire behavior that is more difficult to control (Turner et al., 2019; Schoennagel et al., 2017; Stevens et al., 2014; Shvidenko and Schepascheko, 2013). While globally, the length of fire season has increased by ~19% from 1979 to 2013, the increase in fire season has been even greater in the western US (Jolly et al., 2015), and has been closely tied to temperature, drought, and anthropogenic climate change (Abatzoglou and Williams 2016; Marlon et al., 2012; Westerling et al., 2006). Aggressive fire suppression techniques have also

led to an accumulation of fuels in drier forests previously adapted to frequent low-severity fires that reduced less fire-resistant vegetation. The fuel-build up in these dry forests drives more intense fires and, potentially, conversion into non-forest ecosystems (Seidl et al., 2016). In some moister forests adapted to long fire return intervals, the conditions for major fire activity appear to be occurring with greatly increased frequency due to anthropogenic climate change (Turner et al., 2019). The expansion of the WUI increases wildfire threats to people, homes, and infrastructure and fundamentally changes the tactics and cost of fire suppression; accounting for as much as 95% of fire suppression costs (US Department of Agriculture, Forest Service, 2015). Prescribed fires, and reducing aggressive fire suppression techniques are options to remedy the situation. In particular, combining fuel consumption and emission factor data suggests that prescribed fires produce about 18 times less PM pollution per unit area burned than wildfires (Liu et al., 2017; Sect 4.4). Prescribed fires can reduce hazardous fuels under safe conditions when smoke is largely directed away from most populated areas and they are a major, successful component of land management in the southeast US. However, recent research suggests that in the western US more prescribed fire can reduce wildfire pollution increases and benefit safety in the WUI, but not enough prescribed burning can be done to eliminate future increases in wildfire pollution (Schoennagel et al., 2017). Due to expected wildfire increases and to guide the recommended increased implementation of prescribed fires, robust models of smoke production, transport, and chemistry are increasingly needed to understand the impacts of all fires on air quality, visibility, and climate.

Modeling fire and smoke physics is challenging, especially for wildfires. Wildfires can burn day and night (Saide et al., 2015; Vermote et al., 2009) for months in complex and variable fuels emitting smoke from multiple, rapidly changing locations with injection altitudes ranging

over time from downslope flow (Bertschi et al., 2003) to the lower stratosphere (Herron-Thorpe et al., 2014; Fromm et al., 2000; Stocks et al., 1996). Complex downwind terrain influences transport winds and traps smoke (Wagenbrenner et al., 2016). Emissions are thus subjected to a wide range of dispersion scenarios including: injection into the upper troposphere or lower stratosphere with or without pyrocloud formation (Peterson et al., 2017), persistent widespread regional boundary layer haze (Chen et al., 2017), downslope flow of poorly-lofted residual smoldering combustion emissions (Selimovic et al., 2019), entrapment under nighttime-early morning inversions in mountain valleys (Ferguson et al., 2003), fast dilution of point sources in the (warmer, wetter) boundary layer, slower dilution of area sources or in the (colder, dryer) free troposphere (Hodshire et al., 2018), and mid-day mixing down of elevated polluted layers (Xu et al., 2018).

The chemical composition of freshly emitted smoke is complex and may change as fuels or combustion conditions change (Hatch et al., 2017; 2018; Jen et al., 2019). Smoke evolution is also complex and highly dependent on variable atmospheric processing scenarios, but an important suite of smoke species is linked by a connection to UV light. BrC is a current research focus that impacts climate and UV photochemistry. UV light impacts the lifetime of BrC (Fleming et al., 2019), which competes for UV photons with gases like HONO and NO_2, thereby altering photochemistry. UV photolysis of NO_2 is a source of O_3 and NO_2 reacts with O_3 to form NO_3, which may react with NMOG to make BrC and secondary OA (SOA) in general, but O_3 and OH are also important oxidants that can generate BrC and SOA. The amount of NMOG precursors is impacted by gas-particle partitioning, which depends on dilution (Robinson et al., 2007; May et al., 2013) and the emissions of NMOG are higher when the smoldering/flaming ratio increases (Burling et al., 2011). The smoldering/flaming ratio was observed to be higher at

night than during the day in one study (Benedict et al., 2017), and lab simulated fires indicate that BrC emissions are heavily associated with smoldering combustion (Selimovic et al., 2018). NO_2 is produced by flaming combustion or can be from local sources downwind. O_3 is abundant in background air and made during the daytime in smoke plumes (Akagi et al., 2012; Akagi et al., 2013). Secondary nighttime formation of BrC from reactions of fire-emitted NMOGs with NO_3, and potentially O_3 or other pathways is likely. Stockwell et al., (2015) showed that smoldering combustion of biomass releases large amounts of monoterpenes, furans, cresol, etc., all of which can react quickly with NO_3 and form UV-absorbing organic nitrates that have potential to become condensed phase chromophores (BrC) as eventual products (Brown et al., 2013) and observations of nighttime smoke impacting the Colorado Front Range also showed high levels of these same precursors (Gilman et al., 2015). Further, OA in BB plumes intercepted at Mt. Bachelor Observatory was more oxidized after night time aging (Zhou et al., 2017). A significant amount of uncertainty in isolating and evaluating the optical properties of BrC and its overall radiative impact remains difficult to accurately assess, as BrC emissions are typically mixed with co-emitted BC and non-absorbing OA, which can result in some measurement difficulties (Wang et al., 2017; Pokhrel et al., 2017). Nonetheless, several studies have found that including BrC in climate models suggests that net radiative forcing of biomass burning would move in a positive direction (Graber and Rudich, 2006; Ervens et al., 2011; Wang et al., 2014; Laskin et al., 2015; Wang et al., 2017; Feng et al., 2013; Jacobsen, 2014; Saleh et al., 2014; Forrister et al., 2015). This is important, especially in association with warming-induced increases in fire activity (Westerling et al., 2006; Feng et al., 2013; Doerr and Santin, 2016; Bowman et al., 2017).

Other important smoke evolution issues include the net result of competition between OA evaporation and SOA formation as well as the impact of smoke on surface O_3 levels. Airborne and laboratory studies of SOA and lab studies of BrC evolution so far provide variable outcomes and no clear guidance on the factors controlling smoke evolution (Yokelson et al., 2009; Cubison et al., 2011; Tkacik et al., 2017; Vakkari et al., 2018; Garofalo et al., 2019; Fleming et al., 2019; Ahern et al., 2019). More importantly, they do not provide specific or typical smoke characteristics in heavily-impacted surface locations, which are needed to evaluate model predictions of surface air quality. While airborne studies provide initial near source emissions and the first few hours of plume evolution at high altitude in vigorously lofted plumes (Garofalo et al, 2019; Liu et al., 2017; Collier et al., 2016; Akagi et al., 2013; Akagi et al., 2012; Yokelson et al., 2009; Sedlacek at al., 2018), surface measurements downwind of the source, especially in valleys at low elevations, can document specific and typical smoke air quality impacts on populated areas. Ground-based measurements can provide a top-down evaluation of net regional surface impacts using ratios between inert tracers (e.g. $\Delta BC/\Delta CO$) sensitive to the flaming/smoldering ratio at the source, ratios including evolving species (e.g. $\Delta O_3/\Delta CO$, $\Delta PM/\Delta CO$, $\Delta BrC/\Delta CO$) sensitive to secondary O_3/aerosol evolution, and time series or hourly-average values for inert tracers (e.g. BC, CO) sensitive to assumed emissions production and assumed diurnal profiles of fuel consumption as well as meteorology. Thus, constraining these variables is critical to accurately assessing climate and air quality impacts especially as they relate to model forecasting of smoke downwind in populated areas. Such surface measurements, which are also needed to understand the interaction of regional smoke with non-BB sources, are still relatively rare (Selimovic et al., 2019).

To address the above issues, we began measurements of wildfire smoke impacting the Missoula valley (a western urban center downwind of numerous wildfires) in August-September 2017 obtaining 500 hours of data (Selimovic et al., 2019). In this study we continued the measurements, with an expanded suite of instruments, for another 517 hours of smoke impacts during August-September 2018. Two photoacoustic extinctiometers (PAXs), a Fourier-transform-infrared spectrometers (FTIRs), and added in 2018, an O_3 monitor, a NO_x monitor, and a second FTIR were used to characterize the smoke that entered the valley. A Montana Department of Environmental Quality (DEQ) BAM 1020 measured $PM_{2.5}$ (particulate matter ≤ 2.5 µm in diameter). The PAXs provided measurements of scattering and absorption at two wavelengths (401 nm, 870 nm), BC mass, contributions to UV absorption nominally due to BrC, and derivations of the single scattering albedo (SSA), absorption Ångström exponent (AAE), and scattering Ångström exponent (SAE). The optical property measurements can be normalized to the aerosol mass data to probe multi-step, bottom-up calculations of climate-relevant aerosol optical properties that start with aerosol mass. Further, combining carbon monoxide (CO) measured by our FTIRs with the other species measured (BC, $PM_{2.5}$) produced ratios relevant to models, as mentioned above. Finally, we measured smoke impacts on O_3 and combining our NO_2 and O_3 measurements allowed us to calculate the NO_3 production rate and probe the potential NO_3 contribution to in-situ nighttime BrC formation. The main goals of our study are to assess the relevance of lab and airborne field measurements, the representativeness of emissions inventories, and guide model development by documenting actual surface level characteristics of aged/transported wildfire smoke in a representative, regional population center. We also interpret and assess the interannual variability of our results by comparing them to our previous (2017) measurements of ambient smoke in the Missoula valley (Selimovic et al., 2019).

2 Materials and Methods

2.1 Site Descriptions

Our smoke monitoring site remained unchanged between 2017 and 2018, and is described in more detail in Selimovic et al., 2019. Nonetheless, we reiterate a few key details here. Trace gases and particles were measured through co-located inlets at the University of Montana (UM), ~12.5 m above the ground through the window of our laboratory on the top floor of the Charles H. Clapp building (CHCB), which is ~1.1 km from the nearest road that gets significant traffic during summer recess. $PM_{2.5}$ measurements were made by the Montana DEQ via a stationary $PM_{2.5}$ monitor located in Boyd Park, Missoula ~3.2 km southwest of the CHCB, with both sites being located in the Missoula valley proper. CO, BC, and $PM_{2.5}$ were highly correlated during smoke events and usually at low levels otherwise confirming minimal anthropogenic influence on our smoke data for these species. However, any spikes in BC or CO without PM enhancements or visible smoke and often with high NO/NO_2 ratios were considered anthropogenic and removed from the analysis.

2.2 Instrument Details

2.2.1 Fourier transform infrared spectrometers

Measurements of carbon monoxide (CO) were made using two co-located FTIRs. The first FTIR (Midac Corp., Westfield, MA), used during the 2017 smoke measurements houses a Stirling cycle cooled mercury-cadmium-telluride (MCT) detector (Infrared Associates, Stuart, FL: Ricor USA Inc, Salem, NH) interfaced with a 17.22 m path closed multipass White cell (Infrared Analysis, Inc., Anaheim, CA) that is coated with a halocarbon wax (1500 Grade, Halocarbon Products Corp., Norcross, GA) to minimize surface losses (Yokelson et al., 2003), and is described in more detail elsewhere (Selimovic et al., 2019). The second FTIR, added during the 2018 monitoring period, consists of a Bruker Matrix-M IR Cube spectrometer with an

MCT Stirling cycle cooled detector interfaced to a permanently aligned 78 m closed uncoated multipass White cell (IR Analysis, Inc.) that is more sensitive due to the longer path length. Ambient air was drawn into both systems at ~6 L min^{-1} via a downstream IDP-3 dry scroll vacuum (Agilent Technologies) pump using two respective 0.635 o.d. corrugated Teflon inlets co-located with the other inlets. Spectra for both FTIRs were collected at a resolution of 0.50 cm^{-1}, but the second only covered a frequency range of 600-3400 cm^{-1}. A time resolution of approximately 5 minutes was more than adequate for both systems and sensitivity was increased by co-adding scans at their respective frequencies. Although the systems were designed for source measurements, and are described elsewhere in more detail (Akagi et al., 2013; Stockwell et al., 2016a, b, Selimovic et al., 2019), both FTIRs are convenient for ambient monitoring because the Stirling cooled detectors do not require refilling of liquid nitrogen allowing mostly autonomous operation. Additionally, the use of two FTIRs allowed for intercomparison of trace gas measurements, and served to supplement data in instances where it might have been missing from the other system (i.e. if one system shut down unexpectedly). Although both FTIRs can measure an extensive range of trace gases from sources, in the relatively dilute smoke impacting Missoula during 2018, most gases were retrieved with insufficient signal to noise or influenced by too many sources (e.g. CH_4, CO_2) to be readily interpretable, thus, only CO is reported. To summarize in context; in 2017 many of the wildfires were close to Missoula, CO levels reached almost 3000 ppb, and a number of gases (such as ethylene, ammonia, methanol, etc.) were often above the FTIR detection limits of several ppb. In 2018, the wildfires were further from Missoula, CO levels remained below ~800 ppb, and only excess CO was measured with sufficient signal to noise to clearly dominate background variability. CO mixing ratios were quantified by fitting a region of the mid-IR transmission spectra with a synthetic calibration

nonlinear least squares method (Griffith, 1996; Yokelson et al., 2007) applying the HITRAN spectral database (Rothman et al., 2009). Excess CO was virtually identical on the two systems. Uncertainties in excess CO mixing ratios in smoke (ppmv) varied by spectrum and were dominated by uncertainty in the reference data (<5%) and the background (~5-20 ppb).

2.2.2 Ozone Monitor

The 2B Technologies (Boulder, CO) model 211 O_3 monitor is a dual-beamed 254 nm photometer that uses the reaction between ambient O_3 and NO generated in situ by upstream photolysis of added nitrous oxide (N_2O), to quantify ozone by conventional UV photometry without the issues affecting conventional O_3 scrubbers. Light intensity measurements are made with O_3 present (I) and with O_3 selectively removed by NO (I_0), and the O_3 concentration is then calculated using the Beer-Lambert Law. O_3 calibrations were run using a model 306 O_3 calibrator (Birks et al., 2018a, 2B Technologies). Some UV-absorption O_3 monitors remove O_3 by passing the sample air flow through a solid scrubber, which ideally would destroy O_3 but pass mercury and any UV-absorbing compounds. In practice, however, mercury and aromatic compounds such as benzene, toluene, xylene, etc., can adsorb or react at the solid-phase scrubber surface. As a result, traditional O_3 monitors may report erroneously high O_3 values by up to a few ppb in some cases (2B Technologies, https://twobtech.com/docs/tech_notes/TN040.pdf). A 2 L min^{-1} sample flow of ambient air was drawn into the instrument through a 0.638 cm o.d. FEP inlet (~12.5 m above ground level) and a Teflon filter (Savillex, 47 mm 5-6 micron) to remove particles, which was replaced every 2 weeks or when visual signs of filter loading were apparent. O_3 was sampled at 1 minute intervals, but the data were averaged to 5 min for final analysis to match the time resolution of the FTIRs. Resolution of the 211 O_3 monitor is 0.1 ppb, with a limit of detection (2σ) of 1.0 ppb for a 10s average.

2.2.3 NOx Monitor

The 2B Technologies model 405 nm NO_x monitor measures nitrogen dioxide (NO_2) directly by absorbance at 405 nm and nitric oxide (NO) after conversion to NO_2 with ~100% efficiency using the reaction of NO with O_3. Because NO_2 has a lower absorption cross-section

than O_3, a folded cell with corner mirrors is used to produce a long absorbance path of ~2 m to achieve approximately similar sensitives for NO_2 as for ozone (Birks et al., 2018b). Sample air is continuously drawn through the instrument by an internal pump at a flow rate of ~1.5 L min^{-1} through 0.638 cm o.d. FEP tubing co-located with the other inlets and a Teflon filter (Savillex, 47 mm 5-6 micron) to remove particles. The filter was replaced every ~2 weeks or when visual signs of filter loading were apparent. The instrument was "zeroed" on multiple occasions using zero air that was humidified to match ambient RH with nafion tubing. This ensures the refractive index in the cell and the path length do not change. The measurement of light intensity in the absence (I_0) and presence (I) of NO_2, allows the NO_2 concentration to be calculated using the Beer-Lambert Law. NO is quantified by measuring the decrease in light intensity while adding O_3 to convert NO to NO_2. A small, ~1-2%, loss of 405 nm absorbance from the reaction of NO_2 with O_3 is corrected in the firmware (Birks et al., 2018b). NO_x is computed from NO plus NO_2. NO_2, NO, and NO_x were measured/logged at 1 minute time resolution, but the data were averaged to 5 min for final analysis to match the time resolution of the FTIRs. Accuracy of the NO_x monitor was limited primarily by the drift in manual zeros of 0.75 ppb (1σ).

2.2.4 Photoacoustic extinctiometers (PAX) at 870 and 401 nm

Particle absorption and scattering coefficients (B_{abs}, Mm^{-1}, B_{scat}, Mm^{-1}) were measured directly at 1 s time resolution using two photoacoustic extinctiometers (PAX, Droplet Measurement Technologies, Inc., Longmont, CO; Lewis et al., 2008; Nakayama et al., 2015), which were then used to derive the single scattering albedo (SSA) at 401 and 870 nm and the absorption and scattering Ångström exponents (AAE, SAE). Details for calculating SSA and AAE, as well as operation and limitations of the PAX instrumentation are described in detail elsewhere (Selimovic et al., 2019), but we reiterate a few key points for the 2018 monitoring

period. The main PAX sample line was 0.638 cm (o.d.) Cu tubing co-located with the other inlets. A 1L min^{-1} aerosol sample flow was drawn through each PAX using a downstream IDP-3 scroll vacuum pump (Agilent Technologies). A scrubber and dryer removed absorbing gases and kept relative humidity below 30%, as described in detail by Selimovic et al., 2019. The 1 Hz PAX data were averaged to 5 minutes and matched the time resolution used by the other instruments. In 2018, we switched from a 1.0µm cutoff cyclone to 2.5µm cyclone.

We directly measured aerosol absorption (B_{abs}, Mm^{-1}) and calculated BC concentration (µg m^{-3}) at ambient temperature and pressure using the literature and manufacturer-recommended MAC (4.74 ± 0.63 m^2 g^{-1} at 870 nm) (Bond and Bergstrom, 2006), but note that the BC mass can be adjusted using a different MAC value. To a good approximation, sp^2-hybridized carbon (including BC) absorbs light proportional to frequency (Bond and Bergstrom, 2006). Thus, the B_{abs} contribution from BC at 401 nm can be derived from ~2.17 times B_{abs} at 870 nm (assuming an AAE of one, negligible BrC absorption at 870 nm, and minimal lensing effects). Any additional B_{abs} at 401 nm can be assigned to BrC (B_{abs}, BrC) with this attribution subject to limitations discussed elsewhere (Pokhrel et al., 2016; 2017; Lack and Langridge, 2013; Lack and Cappa, 2010).

Uncertainty in PAX absorption and scattering measurements has been estimated to be ~4-11% (Nakayama et al., 2015), but a few sources of uncertainty, for instance, MAC increases due to coatings, particle losses in the dryer or scrubber, and truncation error in the nephelometer may all contribute. Mie calculations suggest scattering could be underestimated by 1% at 870 nm and 2.5% at 401 nm due to truncation error. This would reduce MSCs (Section 4.6) and typically a 1% reduction in scattering would imply approximately a tenth of a percent of value underestimation in SSA. Particle losses would reduce scattering, absorption, and derived BC, but

have no impact on SSA, SAE, or AAE. We found that adding an extra scrubber reduced scattering and absorption at both wavelengths by 7±5% on average and adjusted the data upwards by 13% to account for both the dryer and scrubber. Unlike particle losses, an increased MAC due to "lensing", mentioned above, could inflate BC values by up to ~30% (Pokhrel et al., 2017).

2.2.6 Montana Department of Environmental Quality $PM_{2.5}$

The Montana DEQ uses beta attenuation monitors (Met One Instruments, Model BAM-1020) in accordance with US EPA Federal Equivalent Methods (FEM) for continuous $PM_{2.5}$ monitoring, which is described in more detail in Selimovic et al., 2019. Critically, however, combining $PM_{2.5}$ measurements with our scattering and absorption measurements from the PAX allows us to derive values for MAC and MSC at both wavelengths, which is discussed more in Section 4.6. Current and archived air quality data for the state of Montana can be accessed using the following link: http://svc.mt.gov/deq/todaysair/.

2.2.7 Emission ratios (ERs) and downwind enhancement ratios

We used the time series of our mixing ratios or concentrations for each analyte measured to derive other values that are broadly useful for both study comparisons and integration in local to global chemistry and climate models. In order to do this, we produced emission ratios (ERs) and enhancement ratios. The calculation of these two types of ratios is identical, but an emission ratio is only the appropriate term for a ratio measured directly at a source or further downwind for a relatively inert species such as BC or CO. An excess amount, denoted by "ΔX" for each species X is calculated for all species measured by subtracting the comparatively small background based on a sloping baseline from before to after a smoke impact. Then, for example, the ratio for each species relative to CO (ΔX/ΔCO) is the ratio between the sum of ΔX over the

entire smoke impacted period relative to the sum of ΔCO over the entire smoke impacted period. Mass ratios to CO were calculated for BC and PM when enhancement above background levels for each smoke impacted period were exhibited.

3 Overview of smoke impacts

Figure 1 shows the hourly average concentrations for $PM_{2.5}$, AAE derived from 5 minute averages of B_{abs} at 401 and 870 nm, and 5 minute average concentrations or mixing ratios of BC, CO, NO_x and O_3 from 7 August to 10 September 2018. Individual episodes of smoke from various locations are shown in greater detail in figures S1-S5. In Fig. 1, wildfire smoke episodes are represented by the yellow shaded area and were identified by large simultaneous enhancements in CO, BC, and $PM_{2.5}$, for sustained periods (≥ 6 hours) when average $PM_{2.5}$ was consistently elevated above the 12.5 μg m^{-3} EPA standard for "good" air quality and smoke was visibly present. The very high correlation of CO and BC to $PM_{2.5}$ suggests that the smoke was well mixed on the spatial scale that separated the $PM_{2.5}$ and UM equipment. NO_x has a relatively short lifetime in smoke plumes (Akagi et al., 2012), thus cases where the correlation of NO_x and CO was high, and there was no smoke visibly present were considered anthropogenic in origin and were not included in the analysis. To investigate the wildfire sources contributing to each episode we used a combination of meteorological observations, geostationary satellite observations, near-surface smoke according to the High Resolution Rapid Refresh (HRRR) model (https://rapidrefresh.noaa.gov/hrrr/), and back trajectory calculations utilizing the National Oceanic and Atmospheric Administration (NOAA) Air Resources Laboratory Hybrid Single Particle Lagrangian Integrated Trajectory (HYSPLIT; Stein et al., 2015; Draxler, 1999; Draxler and Hess, 1997, 1998). Due to the complex local topography and micrometeorology, the combination of these methods can only suggest a likely smoke origin and cannot provide an

exact smoke age, but it is helpful in informing our results in terms of transport and smoke age, which was between several hours and up to two days old.

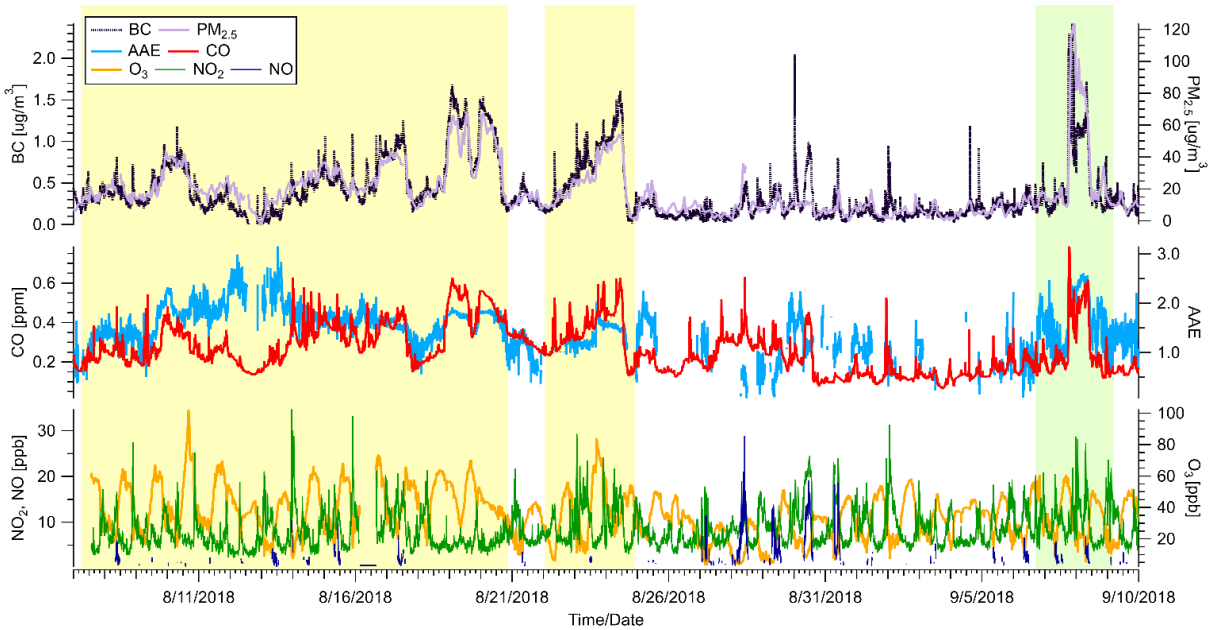

Figure 1. Time series of hourly PM, hourly derived AAE, 5-minute BC, CO, NO_x, O_3 measurements from Missoula. Sections shaded in yellow represent wildfire smoke impacted periods. Sections shaded in green represent prescribed fire smoke impacted periods. Unshaded areas represent anthropogenic impacts and were not included in the analysis.

We also present measurements for one "summer" prescribed fire impact (shaded in green), for which the origin is known, and which represents smoke ~3 hours old. The prescribed fire burned over 100 hectares, in a Lodgepole pine dominated ecosystem, and was a stand-replacing fire, producing smoke likely more similar to that from naturally occurring wildfires than is the case for the more common lower-intensity prescribed fires that focus on clearing out understory fuels while preserving overstory trees.

4 Results and discussion

4.1 O_3

Numerous airborne studies have documented O_3 formation in smoke plumes (Akagi et al., 2013; Liu et al., 2016) and several studies have suggested that wildfires can also lead to an

increase in the amount of ground-level O_3 (Brey and Fischer, 2016; Liu et al., 2016; Morris et al., 2006). For instance, wildfire emissions enhanced average summertime monthly mean O_3 by 2-8 ppb in the Intermountain West (Jaffe et al., 2018). In another study boundary layer O_3 showed more influence from local, continental or marine sources, while observations at high elevation sites (1.5—3.0 km above sea level) showed greater influence from large-scale downward mixing of free tropospheric air and from transport of photochemically aged plumes from wildfires (Ambrose et al., 2011). In general, the total amount of O_3 in an area is a complex combination of the relative amounts of NMOGs and NO_x, meteorological conditions supporting local production, and the amount of O_3 present in background/transported air (Lindaas et al., 2017). In this section we investigate the effect of both dilute, aged (up to several days) wildfire smoke and thicker, moderately fresh (~3 hour old) prescribed fire smoke on O_3 levels in Missoula by comparing the amount of O_3 present in typical background ambient conditions during clear sky to smoke impacted days.

The two largest mixing ratios in our five-minute O_3 data are associated with aged smoke from Idaho (102 ppb, Fig, S1) and Washington (82 ppb, Fig. S4). O_3 values associated with aged smoke from Idaho occurred during higher than normal daily maximum temperatures (38ºC), but the O_3 values associated with aged Washington smoke were in cooler air in comparison (25º C). Although higher temperatures are associated with higher O_3 values, the fact that these peaks are about 45 and 25 ppb higher, respectively, than the typical summertime 5-min O_3 maximum in clean air suggests that aged smoke (and the meteorological conditions that favor smoke production) can be associated with significant enhancements in O_3 exposure. To explore this systematically we used hourly average O_3 data. Diurnal cycles for O_3 in each case are plotted in

Figure 2a, and were compiled by computing hourly averages from five minute O_3 data, for each hour of the day over the duration of the study.

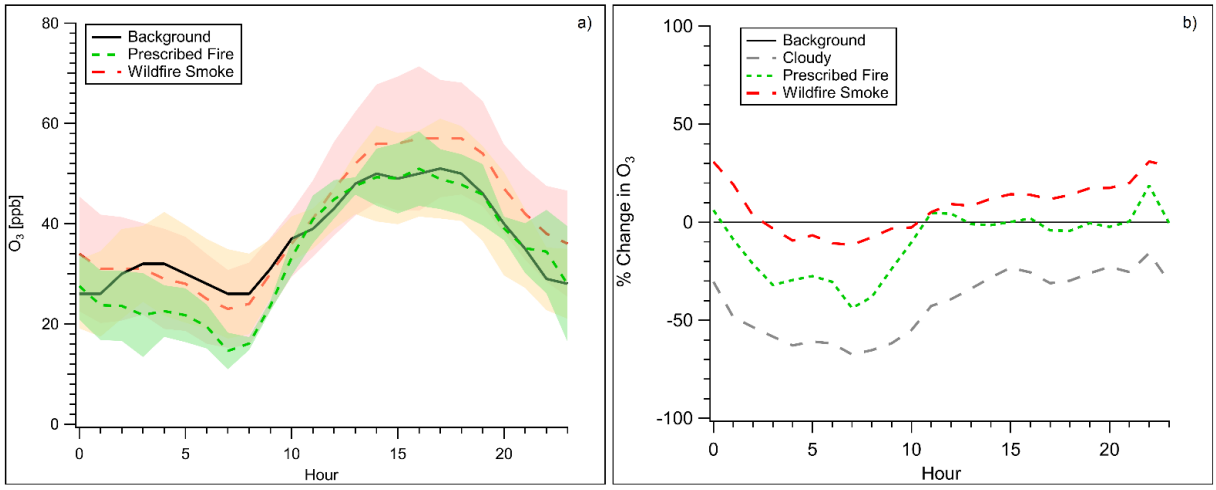

Figure 2. Panel (a): A comparison of the average diurnal cycle of O_3 during clear-sky, wildfire (aged, up to several days) smoke impacted periods, and prescribed (3 hours old) smoke impacted periods. Shaded area in yellow represents ±1σ for clear-sky background values. Shaded area in green represents ±1σ for prescribed fire smoke values. Shaded area in red represents ±1σ for wildfire smoke values. Panel (b): Percent change relative to the average diurnal cycle of O_3 during wildfire smoke impacted, prescribed fire smoke impacted, and cloudy days.

Clear sky background days and cloudy days were verified using historical weather data and satellite retrievals. Although we acknowledge that O_3 exhibits a temperature dependence and typical background concentrations vary seasonally, background (smoke-free) hourly-average O_3 mixing ratios throughout the duration of our study remained fairly consistent around 50 ± 5 ppb during the afternoon and 30 ± 5 ppb at night throughout the monitoring period. “Background” O_3 was defined as the average O_3 during days not impacted by smoke or clouds over the duration of the study. Figure 2a shows increases in O_3 diurnal cycle mixing ratios throughout all periods of the day during wildfire smoke-impacted times, compared to the average clear sky background diurnal cycle. The O_3 mixing ratio across the entirety of the diurnal cycle was, on average, ~6 ppb (15%) higher during wildfire smoke-impacted periods than during average cloud-free and

clear sky background periods. Conversely, the O_3 mixing ratio across the entirety of the diurnal cycle was on average ~4% lower during the prescribed fire (thick smoke) impacted period than clear sky background conditions; most likely due to reduced photochemical production associated with high BrC levels. We observe the largest relative enhancements of O_3 during aged, wildfire smoke impacted periods after sunset and persisting for several hours after midnight with the mixing ratio of O_3 on average, ~9 ppb (23%) higher than corresponding average smoke-free periods. This suggests that aged smoke could prolong the O_3 lifetime in the dark or that wildfire smoke enhanced daytime O_3 formation upwind of Missoula more than in Missoula, and these air masses arrived in Missoula after dark, with the latter case implying substantial regional enhancement in O_3 due to wildfire smoke. Combining field observations during the Southeast Nexus (SENEX) campaign with chemical box modeling using laboratory derived BB emission factors (EFs) measured as part of the Fire Influence on Global and Regional Environments (FIREX) campaign (Selimovic et al., 2018; Koss et al., 2018), Decker et al., (2019) showed that although a change in the ambient concentration of O_3 has little effect on the relative reactivity of nighttime oxidants such as NO_3 and O_3, including night-time O_3 oxidation in photochemical models should still be critical, as it has potential to affect next day photochemistry. For instance, Decker et al., (2019) reported that while the nighttime oxidation of NMOGs produced by BB for some fuels is dominated by NO_3, in some cases, oxidation by O_3 remains significant (e.g. 43% for ponderosa pine fires). An important note however is that these model results are lower limits that are applicable to the center of a young BB plume and do not include later dispersion, where non-BB sources of NO_x mixed with O_3 downwind leads to additional depletion of NMOGs. Mixing effects have potential to be even more significant in urban areas impacted by BB plumes. I.e. urban sources of NO_x mixed with ambient background

O_3 and elevated O_3 formed in aged plumes can contribute to additional oxidation and depletion of BB produced NMOGs.

4.2 NO_x

NO_x (the sum of NO and NO_2) is effectively a precursor to two main atmospheric oxidants (O_3 and NO_3) and its chemistry is related to BrC as noted earlier. We note that for the majority of our sampling period, (≥ 95% of the time), our NO values were below detection limits. Further, when we did briefly measure NO during smoke impacted periods, the NO/NO_2 ratio was about ~0.23. Thus, our NO_x measurement is mostly a measurement of NO_2. NO_x/CO is usually about 1-2% in fresh forest fire plumes and after 2-3 hours it is converted chiefly to PAN and particle nitrate (Akagi et al., 2011, 2012, Liu et al., 2016, 2017). The 5-minute data shows NO_2 present as peaks up to ~30 ppb during aged smoke impacts, which is more than 1-2% of CO confirming a local source (Figs S1-S5). Some of the largest NO_x peaks occur after dark before midnight, and NO_2 peaks are dramatically anti-correlated with O_3, which is consistent with high NO_3 production rates (Figs S1-S5) We investigate the effect of both wildfire and prescribed fire smoke in an analysis identical to the analysis done for O_3, whereby diurnal cycles of NO_x were plotted by computing hourly averages from 5-minute NO_x data, for each hour of the day over the duration of the study. Figure 3 shows that were no significant changes to the diurnal cycle of typical “background” concentrations of NO_x during either aged wildfire-smoke impacted periods or moderately fresh prescribed fire impacts. For the duration of the study, NO_x for both of the latter periods remained within the range of typical ambient concentrations, again suggesting our measured NO_x is likely the result of local emissions.

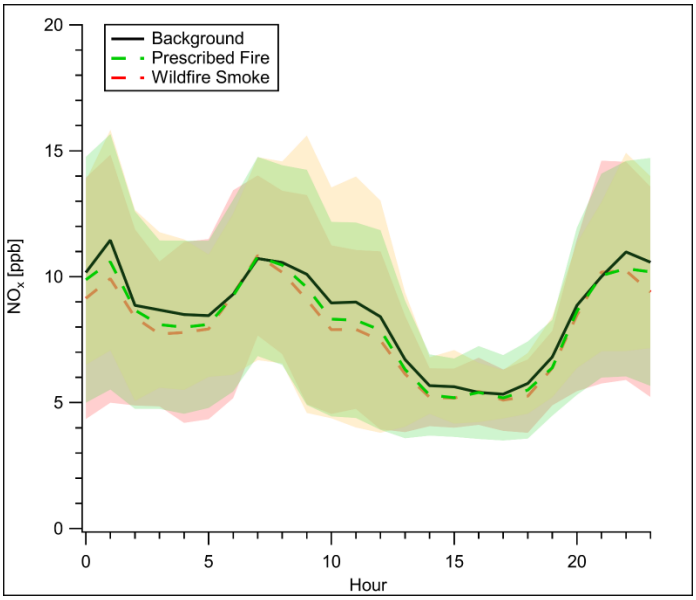

Figure 3. Average hourly diurnal cycles of NO_x measured in the Missoula valley calculated from 1 hour averages of 5-minute data. Shaded area in yellow represents ±1σ for background values. Shaded area in green represents ±1σ for prescribed fire smoke values. Shaded area in red represents ±1σ for wildfire smoke values.

The trend in the hourly average diurnal cycle loosely resembles a traffic source peaking during morning traffic and afterwards diluting. Plume dilution and rapid loss of NO_x as smoke is transported away from a fire suggests slowing of O_3 formation downwind. However, several studies show that urban sources of NO_x mixed with biomass burning plumes can lead to an increase in O_3 (Jacob et al., 2010; Lee et al., 2009), and the highest O_3 formation rates in smoke plumes sampled by Akagi et al., (2013) occurred when a plume was mixed with urban emissions. Thus, our measurements of urban NO_x are likely critical to explaining some portion of the daytime O_3 enhancements discussed in the previous section.

4.3 NO_3 Production

$P(NO_3)$ is the instantaneous formation rate of NO_3 through reaction of NO_2 and O_3 calculated via the following: $P(NO_3) = K_{NO3}[NO_2][O_3]$ ($k=3.2 \times 10^{-17}$ cm^3 $molec^{-1}$ s^{-1} at 298 K; Burkholder et al., 2015). Reactions of NO_3 with many NMOGs are efficient and can lead to the

production of organic nitrates and secondary organic aerosol (Brown et al., 2012), altering nighttime oxidative budgets. Several studies show NO_3 leading to formation of secondary BrC aerosol, suggesting that nighttime oxidation may be a significant source of BB derived BrC, which has potential to affect next-day photochemistry (Palm et al., 2017; Laskin et al., 2015; Mohr et al., 2013; Iinuma et al., 2010). Using laboratory emission factors measured at the Missoula Fire Sciences Lab in 2016 (Selimovic et al., 2018; Koss et al., 2018), Decker et al. (2019) modeled an NO_3 production rate ($P(NO_3)$) of 1 ppbv hr^{-1} in fresh plumes, and here we present complementary evidence of high $P(NO_3)$ occurring in aged smoke. Although NO_3 is rapidly photolyzed during the day, we calculate $P(NO_3)$ during night and day, because high NMOG concentrations and suppression of photolysis in thick smoke might make reactions of NO_3 competitive with photolysis. Figs. S1-S5 show numerous $P(NO_3)$ peaks above 1 ppb/hr and some above 2 ppb/hr. Figure 4 plots high resolution (5 minute) data of O_3 and NO_2 as a function of calculated $P(NO_3)$. Although the highest instances of $P(NO_3)$ were observed during wildfire smoke impacted periods (2.44 ppbv hr^{-1}) (Fig. 4d), on average, $P(NO_3)$ was highest during prescribed fire impacts (Fig 4c).

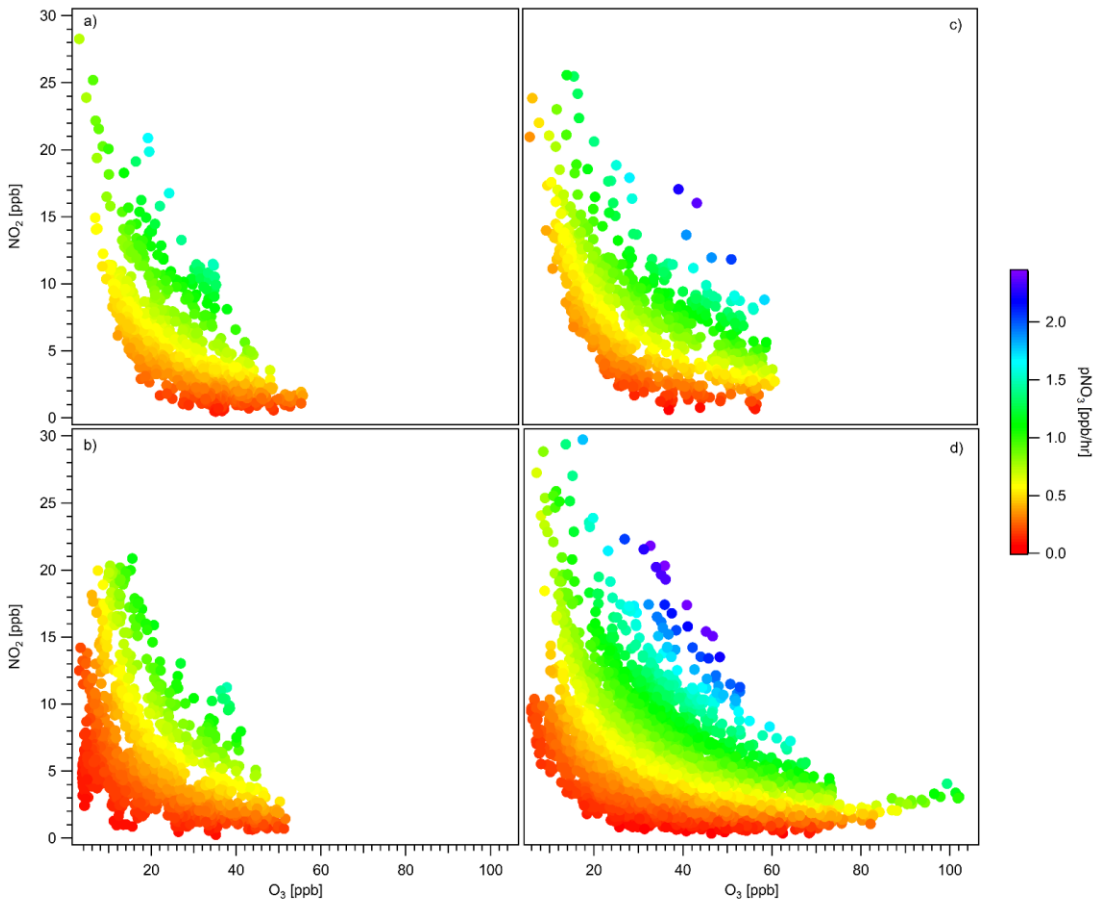

Figure 4. NO_2/O_3 plots colored by pNO_3. Panel (a) represents typical clear sky smoke-free background conditions, panel (b) represents cloudy smoke-free conditions, panel (c) represents prescribed-fire (3 hours old) smoke conditions, panel (d) represents aged (up to several days) wildfire smoke impacted conditions.

The average $P(NO_3)$ for wildfire impacts was 0.57 ppbv hr^{-1}, and the average for prescribed fire impacts was 0.66 ppbv hr^{-1}. In both cases, $P(NO_3)$ is higher than when compared with clear, smoke-free $P(NO_3)$ (0.47 ppbv hr^{-1}) and during cloudy periods (0.35 ppbv hr^{-1}). In Figure 5, we investigate diurnal trends in $P(NO_3)$ by calculating hourly averages from 5-minute data of O_3 and NO_2 and then plotting them as a function of the hour of day. A weak trend shows that high $P(NO_3)$ is driven by large percentage increases in NO_2, which has implications for when/where NO_3 is formed. For example, at the plume source, where BB-NO_2 is abundant, NO_3 production is likely high, as shown in Decker et al., 2019. In addition, our data confirms that

formation of NO_3 in smoke downwind of fires due to "added" NO_2 is also important. This is likely due to non-fire sources of NO_2 (urban or lightning) or NO_2 from the thermal decomposition of fire-generated PAN mixing with enhanced levels of O_3 in aged plumes driving NO_3 production.

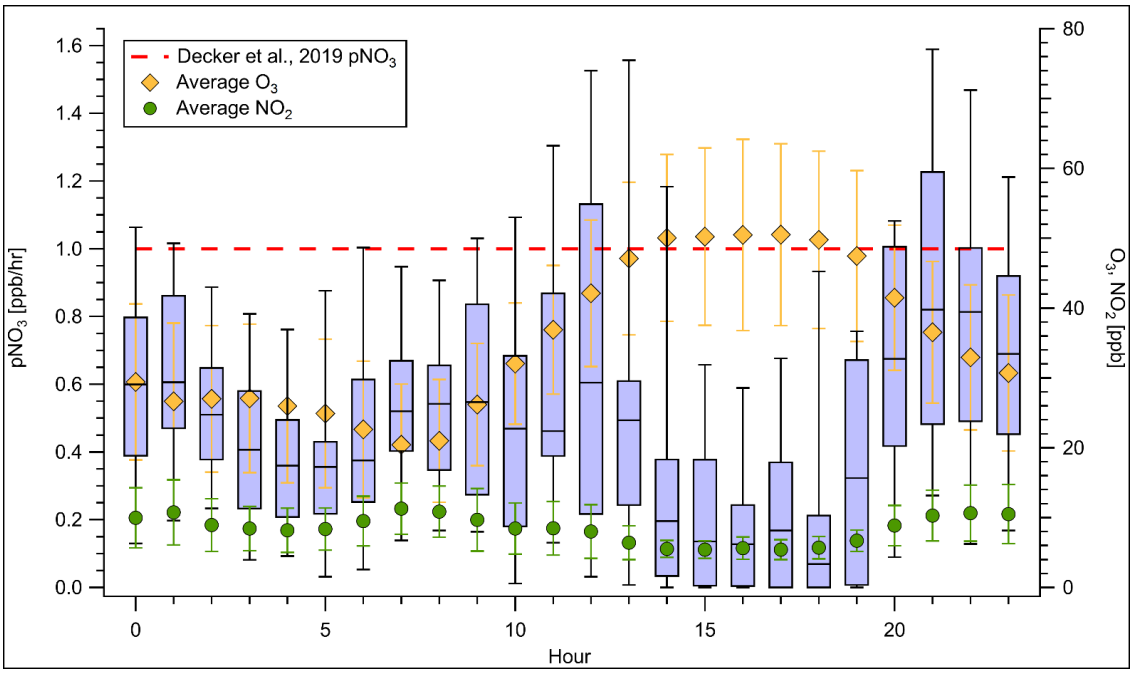

Figure 5. Hourly diurnal box and whisker plot of pNO_3 plotted with hourly diurnal plots of O_3 and NO_2. Values were derived from hourly averages of 5-minute wildfire smoke impacted data. Error bars on O_3 and NO_2 represent 1σ.

4.4 $\Delta BC/\Delta PM_{2.5}$, $\Delta BC/\Delta CO$, $\Delta PM_{2.5}/\Delta CO$

We begin this section with a summary of the importance of the $\Delta BC/\Delta CO$, $\Delta BC/\Delta PM_{2.5}$ and $\Delta PM_{2.5}/\Delta CO$ ratios. Although BC is estimated to be the second strongest global climate warming agent, accurate measurements of ambient BC and BC EFs remains challenging, and aerosol absorption remains a large contributor to uncertainty in models (Bond et al., 2013; Li et al., 2019). CO emissions estimates are in reasonable agreement for western wildfires (Liu et al., 2017), and can be used to derive BC emissions estimates. For example, combining the measurements of these two "inert" tracers into a $\Delta BC/\Delta CO$ ratio can be used with CO emissions

to update BC emissions estimates from wildfires, which could improve model input and further assist in validating current models. In addition, BC is only made by flaming combustion at the fire source, and although its production can differ vary with flame turbulence (Shaddix et al., 1994), the ΔBC/ΔCO ratio can be used as a rough indicator of the fire flaming to smoldering ratio, as demonstrated in Selimovic et al. (2019) Figure 2b. Turning to reactive species, a rough metric for the net effect of secondary formation and evaporation of organic and inorganic aerosol is provided by changes in the ΔPM/ΔCO ratio as smoke ages. However, as referenced in the Introduction, there remains much ambiguity about the factors controlling the evolution of this ratio as smoke is transported downwind, and, in addition, few studies provide this ratio in heavily-impacted surface locations which is critical in assessing model predictions of surface air quality, especially as it relates to impacts on populated areas (Bian et al., 2017; Lim et al., 2019; Ahern et al., 2019; Morgan et al., 2019). BC/PM can also indicate PM evolution and roughly indicate climate impacts.

Table 1 reports our ΔBC/ΔCO, $\Delta PM_{2.5}/\Delta CO$, and $\Delta BC/\Delta PM_{2.5}$ mass ratios for aged wildfire smoke impacts and for the one fresher prescribed fire smoke impact. $\Delta BC/\Delta PM_{2.5}$ ratios were calculated by computing 1 hour averages of 5 minute BC derived from PAX 870 absorption data and then plotted against 1 hour $PM_{2.5}$ data (Fig. S6). ΔBC/ΔCO ratios were calculated using integrated 5-minute data to account for, and maintain the high time resolution. $\Delta PM_{2.5}/\Delta CO$ was derived using the two calculated ratios. We assess our results by comparing them to previous measurements of ambient smoke in the Missoula valley (Selimovic et al., 2019) and to airborne measurements (Liu et al., 2017; May et al., 2014; Sahu et al 2012). Our wildfire ΔBC/ΔCO ratio (0.0026 ± 0.0007) is roughly two times higher in the wildfire smoke measured in this study compared to the 2017 wildfire smoke measured a year earlier by Selimovic et al., (2019), but our

2-yr average (0.0020 ± 0.0007) is just 25% higher than the Liu et al., (2017) airborne study of 2013 western wildfires (0.0016 ± 0.0018).

Table 1. Study-average enhancement ratios (g g^{-1} ratioed to CO) compared to ratios reported in other studies.

Ratio	Fire Type[a]	This Work	Selimovic et al., 2019[b,c]	Liu et al., 2017[d,e]	May et al., 2014[d,f]	Sahu et al. 2012
ΔBC/ΔCO	WF	0.0026 (0.0007)	0.0014 (0.0006)	0.0016 (0.0018)	--	0.0014
	PF	0.0026	--	--	0.006	--
$\Delta PM_{2.5}/\Delta CO$	WF	0.1070 (0.0278)	0.1263 (0.0015)	0.2661 (0.1342)	--	--
	PF	0.165	--	--	0.11 (0.01)	--
$\Delta BC/\Delta PM_{2.5}$	WF	0.0243 (0.0002)	0.0107 (0.0003)	0.0060 (0.0054)	--	--
	PF	0.0157 (0.0011)	--	--	0.048	--

[a] WF stands for wildfire, PF stands for prescribed fire. Wildfire smoke was more aged (up to several days) than prescribed fire smoke (~3 hours).
[b] BC measurements at 1.0 micron cutoff
[c] BC values reported have been adjusted 13% to account for dryer losses in the PAX instrumentation.
[c] PM values reported are $PM_{1.0}$.
[d] Average of Rim Fire and Big Windy Complex. BC data were analyzed for Liu et al., 2017, but not reported.
[e] Values for the Shaver and Turtle fires (prescribed burns in coniferous ecosystem in Sierra Nevada mountains)

While it's difficult to assess the exact reason for the 2017 to 2018 differences, a likely combination of several factors exist to potentially explain them. First, the wildfire smoke impacting Missoula in 2017 was from closer fires, which could enhance impacts of smoke more dominated by smoldering combustion and with lower BC/CO, as shown in Selimovic et al., (2019). Equivalently, assuming BC and CO remain inert during transport, our higher ΔBC/ΔCO ratio in 2018 could be indicative of fire emissions more dominated by flaming combustion, which were lofted by convection and then transported to the Missoula valley. Additionally, the PAX 870, which we use to derive our BC measurements, does not discriminate against any coating effects, so it is possible that our 2018 BC values are more inflated by lensing effects than in the younger 2017 smoke. Switching from a 1.0 µm to a 2.5 µm cyclone would add additional

mass and could potentially lead to larger values in PAX 870 absorption. Even though BB-BC is nearly all sub-micron, other super micron components (micro-char, dust) may absorb weakly and cause larger calculated values of BC (Han et al., 2009; Clarke et al., 2004). Although the mass in the 1.0-2.5 µm range is thought to be a small part of the total mass (Reid et al., 2005a Fig. 2), the size range difference does affect data interpretation. In Selimovic et al. (2019), we estimated that western US wildfires emit 7.3 ± 3.3 Gg of BC a year. Using the same method described in that study, but now with two years of data averaged, we update that value to 9.4 ± 4.0 Gg of BC produced by wildfires a year. In addition, our ΔBC/ΔCO average across two years times the EF CO for wildfires measured in Liu et al., (2017) (89.3), suggests an EF BC for wildfires of 0.18 g kg^{-1}. Our ΔBC/ΔCO for the summer-time prescribed fire in coniferous fuels in this study (0.0026) is ~2.3 times less than the ΔBC/ΔCO ratio for fall (November) prescribed fire measurements in western US montane fuels reported in May et al., 2014 (0.006); likely reflecting more smoldering consumption of duff and dead/down fuels in the summer prescribed fire.

Our surface $\Delta PM_{2.5}/\Delta CO$ ratios for aged wildfire smoke across both years (0.1070 in 2018, 0.1263 in 2017) are consistently about half that of fresh wildfire smoke (0.2661) sampled in Liu et al., (2017) and fresh or aged smoke samples acquired at higher altitudes in airborne or mountain-top studies (Collier et al., 2016; Garofalo et al., 2019). However, our lower ratios at the surface are consistent with some aircraft samples acquired at relatively lower elevations and latitudes and likely warmer temperatures (Forrister et al., 2015; Capes et al., 2008). This reinforces the observation from Selimovic et al., (2019) that on timescales up to ~1-2 days, aging and/or higher ambient temperatures at the surface may lead to substantial net OA evaporation. This decrease with age may not occur at high altitude, but significantly reduce downwind surface PM impacts. Our $\Delta PM_{2.5}/\Delta CO$ value (0.165) for the fresher prescribed fire smoke (~3 hours old)

is higher than both our 2017 and 2018 values for aged wildfire smoke, but still significantly lower than the wildfire average from Liu at al. (2017). Our prescribed fire $\Delta PM_{2.5}/\Delta CO$ ratio is higher than the wildfire ratio, but has a similar $\Delta BC/\Delta CO$ ratio (at least for 2018). One potential simple explanation is distance, in that the prescribed fire was closer to the Missoula valley than the wildfires impacting the valley during that same year, and thus experienced less dilution/evaporation. Additionally, lower surface temperatures (8ºC —29ºC) during the time of the prescribed fire impact, in comparison to temperatures during the majority of the wildfire impacts may have been less conducive to PM evaporation (Li and Shiraiwa, 2019). The ~15% higher $\Delta PM_{2.5}/\Delta CO$ ratio for 2017 wildfire smoke in Missoula may reflect younger average smoke age (Selimovic et al., 2019). Our summer prescribed fire $\Delta PM_{2.5}/\Delta CO$ ratio is 50% higher than the ratio reported for fresh smoke from the fall prescribed fires in western montane fuels in May et al., (2014) (0.11), but May et al., (2015) also note that their $\Delta PM/\Delta CO$ decreased by about a factor of 2 after several hours of aging on at least one prescribed fire. Fuel and measurement differences (additional mass in the 1.0-2.5 µm range) mentioned earlier could also both potentially account for some of the higher PM/CO produced by the summer prescribed fire.

We stress that there is now more than 1000 hours of ground-based data suggesting that a typical PM/CO value for aged wildfire smoke at the surface is about half the value in fresh to moderately-aged well-lofted wildfire plumes (Liu et al., 2017; Garafalo et al., 2019; Collier et al., 2016). One airborne wildfire study by Forrister et al., (2015) at lower latitudes and sampling elevations than the other airborne studies is consistent with the downwind net evaporation we apparently observe in Missoula. We also stress that, despite the evidence for PM evaporation during aging, there is strong data supporting the idea that wildfires are “smokier” than spring or fall prescribed fires on a per fuel burned or per area burned basis. Liu et al., (2017) reported that

emission factors for $PM_{1.0}$ ($gPM_{1.0}$/kg fuel burned) burned) are almost 4 times higher in wildfires (27.1 ± 6.1) than spring and fall prescribed fires (7.3 ± 4.2, May et al., 2014). Our 2-year average ΔPM/ΔCO ratio in aged wildfire smoke (~0.117) is ~1.7 times higher than implied for aged, fall western montane prescribed fire smoke (~0.07) based on May et al., (2014; 2015) suggesting that a signal of the difference in initial PM emissions can survive aging. Fuel consumption in spring/fall prescribed fires at the national level is typically 7.2 ± 2.7 Mg ha^{-1} (Yokelson et al., 1997; 2013) as opposed to 34.6 ± 9.9 Mg ha^{-1} on wildfires (Campbell et al., 2007; Santin et al., 2015). Combining the emissions and fuel consumption differences implies that wildfires emit 18 ± 14 times more PM per area burned. Although prescribed fires cannot simply replace all wildfires (Turner et al., 2019; Schoennagel et al., 2017) their potential to reduce the level of wildfire impacts deserves more attention. In addition, incorporating higher wildfire initial emissions and temperature-dependent, post-emission OA evaporation may improve models of wildfire smoke impacts (Nergui et al., 2017).

Our study average $\Delta BC/\Delta PM_{2.5}$ ratio for wildfire smoke in 2018 is roughly double our $\Delta BC/\Delta PM_{2.5}$ ratio for 2017 wildfire smoke (Selimovic et al., 2019), and ~4 times higher than the aircraft average $\Delta BC/\Delta PM_{1.0}$ for 2013 wildfires (Liu et al. 2017; Selimovic et al. 2019). Likely reasons for the higher ratio in 2018 include the possible reasons for a higher BC/CO ratio in 2018 mentioned above: e.g., increased lensing in more aged smoke, transport of more flaming smoke, and (less likely) including other absorbers with the $PM_{2.5}$ cutoff. In addition, BC/PM could be higher in 2018 aged wildfire smoke because of more time (on average) for PM evaporation. OA is the main component of wildfire PM (Liu et al., 2017), so the ΔBC/ΔPM ratio should be similar to the ΔBC/ΔOA ratio, which suggests a “low” MAC in the UV for the wildfire OA (Saleh et al., 2014; section 4.6). Our low ΔBC/ΔPM ratios across both years (~1-2%), along

with high SSA (Sect 4.6), further confirm that wildfire aerosol is overwhelmingly organic and strongly cooling. Our summer prescribed fire $\Delta BC/\Delta PM_{2.5}$ is ~3 times lower than the ratio reported for fall prescribed fires in similar fuels in May et al., (2014), which is likely (as noted above) because drier summer burning conditions enables consumption of fuels (e.g., dead/down, duff) that tend to burn by smoldering, but are too wet to burn as efficiently in spring/fall. While we indicate above that wildfires are likely smokier than spring/fall prescribed fires, which has poor implications for air quality, they also appear to have less positive climate forcing. In any case, again, differences in smoke production and chemistry between wildfires and prescribed fires warrants further research, as more definite conclusions can reinforce land management implications.

4.4 UV-Absorption by BrC and AAE

The AAE is an important aerosol optical parameter used for characterization and apportionment studies. Further, the AAE can be used to separate BrC from BC absorption (Liu et al., 2018), and higher AAEs are correlated with absorption that is more dominated by BrC (Pokhrel et al., 2016; 2017; Selimovic et al., 2018; 2019). A lab study with wildfire fuels found that BrC accounted for ~86% of absorption by particles in the UV (401 nm) on average in fresh smoke (AAE of 3.50) which has implications for UV-driven photochemical reactions of O_3 and the lifetimes of e.g. NO_x and HONO (Selimovic et al., 2019). Satellite AAE retrievals and one airborne study indicate that BrC can have a strong impact in fresh wildfire plumes (AAE 2.8—3.75) and significant, persistent impacts in downwind regional haze/plumes (Hammer et al., 2016; Jethva and Torres, 2011; Forrister et al., 2015). There is variability in BrC attribution methods across studies (Forrister et al., 2015; Pokhrel et al., 2017), but despite this, BrC absorption would decrease the climate cooling calculated for purely scattering OA depending on

its MAC, lifetime, and the amount emitted (Feng et al 2013; Forrister et al., 2015). Furthermore, sources of BrC not directly emitted from BB, including the photo-oxidation of NMOGs need to be considered. However, these complex processes produce BrC with optical properties and lifetime that are not yet comprehensively evaluated. Mixing state, combustion conditions, chemical transformation and photochemical aging are all factors that can influence the absorption of secondary BrC (Tomaz et al., 2018; Wang et al., 2017; Laskin et al., 2015; Wang et al., 2014; Ervens et al., 2011; Graber and Rudich, 2006; Fleming et al., 2019).

In Table 2 we present two years of in situ smoke/haze data from Missoula showing persistent widespread regional impacts of BrC and the associated AAE values. Smoke age is a key factor. In 2017 the episode with the highest AAE (2.88, 77% BrC absorption at 401 nm) was due to smoke from a fire just ~2-4 hours upwind and the 2017 average AAE (for smoke 2-48 hours old) was 1.96 (51% BrC absorption at 401 nm). The 2018 smoke was more aged on average (no nearby wildfires) and had a lower study-average AAE of 1.71 (47% BrC absorption at 401 nm), but the one relatively fresh prescribed fire smoke episode in 2018 had a higher than average AAE of 2.49 (71% BrC absorption at 401 nm).

Table 2. Study-average AAE and %BrC contribution to absorption at 401 nm compared to other studies.

Ratios	Fire Type	This Work	Selimovic et al., 2019	Selimovic et al., 2018[a]
AAE	WF	1.71 (0.04)	1.96 (0.38)	3.31
	PF	2.49 (0.04)	--	
%BrC	WF	46.55 (0.51)	50.72 (12.78)	78
	PF	70.79 (0.42)	--	--

[a] WF stands for wildfire, PF stands for prescribed fire. Wildfire smoke was more aged (up to several days) than prescribed fire smoke (~3 hours).
[b] Lab fires, calculated from the average of wildfire MCE reported in Forrister et al., 2015

Remarkably, despite the large range in episode smoke ages across both years, BrC accounted for roughly 50% of the UV-absorption at 401 nm on average both years. The small

~4% difference in % BrC absorption at 401 nm year to year likely indicates that the decrease after emission in net BrC slows significantly after a few hours. In any case obtaining the same average value for moderately aged smoke two years in a row suggests our regional smoke AAE value (~1.7 – 1.9) is a useful target for model validation, which would be hard to demonstrate in lab or airborne studies.

It is interesting to speculate about the impact of combustion conditions and nighttime effects on multiday aging of BrC. Selimovic et al., (2018) showed that higher AAE in the initial emissions is associated with more smoldering combustion. Relatively more smoldering as demonstrated by the lower ΔBC/ΔCO ratio in 2017 could have contributed to the higher AAE in 2017 (along with differences in smoke age). In addition, wildfires can produce much of their emissions at times of day shortly before or after photobleaching would stop (Saide et al., 2015) and wildfires can have a higher smoldering to flaming ratio at night than during the day (Benedict et al 2017), which would likely enhance emissions of both primary BrC (Selimovic et al., 2018) and BrC precursors. Precursors include monoterpenes, furans, etc., that can react with the major nighttime oxidant, NO_3 to form UV-absorbing organic nitrates. Estimates using current NMOG data strongly suggest that a substantial nighttime secondary BrC source could exist (Stockwell et al., 2015, Gilman et al., 2015, Hatch et al., 2017). I.e. converting even a small fraction of co-emitted NMOGs that are known to react quickly with NO_3 could yield substantial amounts of BrC during dark hours and oxidation of NMOGs by O_3 could also be important, as mentioned earlier in Section 4.1. Our five-minute data shows a potential example of this in Fig. S1. Shortly before 12 AM on 12-August there is a spike in NO_3 production followed by a prominent increase in AAE (from ~1.6 to ~3.0) that lasts until sunrise. The increase in AAE is likely not due to arrival of fresher, usually more concentrated, smoke, which we also commonly

see, since hourly $PM_{2.5}$ is simultaneously decreasing. In Figure 6, we show the diurnal cycle of NO_3 production with %-absorption by BrC at 401 nm. The %-absorption by BrC at 401 nm is slightly enhanced at night and loosely follows the NO_3 production consistent with a role for the effects discussed above. However, with the data available, we can't completely separate the potential effects of nighttime NO_3 reactions, enhanced smoldering emissions, or transport/mixing. Nonetheless, the presence of NO_3 as a major nighttime oxidant in the formation of BrC should be considered, as our high NO_3 production rates in an earlier section (4.3) show.

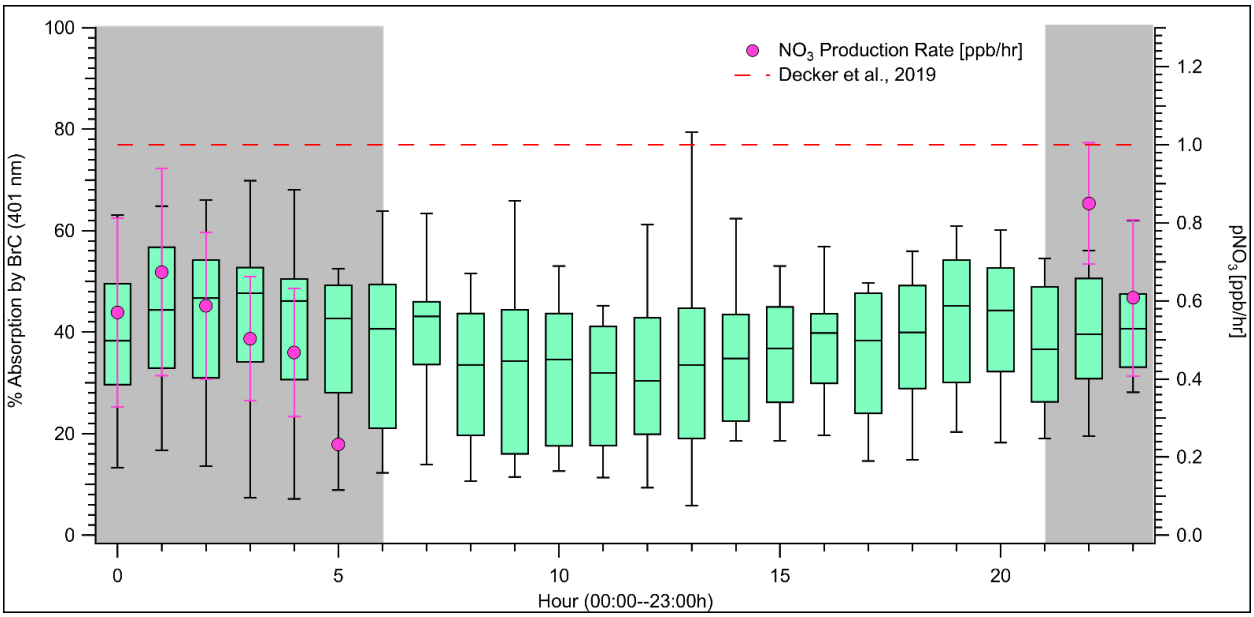

Figure 6. Hourly diurnal box and whisker plot of %-Absorption by BrC calculated from hourly averages of wildfire smoke impacted 5-minute data compared to the night-time (shaded area) hourly average pNO_3. Error bars on pNO_3 represent 1σ.

4.6 SSA, MAC, MSC

Table 3 lists our study average SSAs, MACs, and MSCs. MACs and MSCs can be coupled with $PM_{2.5}$ data to describe the optical properties of aerosol on a per mass basis. Our MAC and MSC values were obtained by plotting 1 hour averages of $B_{scat}401$, $B_{abs}401$, and $B_{scat}870$, $B_{abs}870$ versus the 1 hour $PM_{2.5}$ values in order to calculate an MSC(401), MAC(401),

MSC(870), and MAC(870) (Fig. S7—Fig. S10). In Selimovic et al. (2019), we produced MAC and MSC values by comparing our scattering and absorption measurements measured at a 1.0 µm cutoff to $PM_{2.5}$ data that was available.

Table 3. Study-average MAC and MSC compared to other works.

Parameter	λ (nm)	This Work[a] (WF)	This Work[a] (PF)	Selimovic et al., 2019[b, c]
SSA	401	0.95 (<0.01)	0.95	0.93 (0.01)
	870	0.95 (<0.01)	0.94	0.94 (0.02)
MAC	401	0.43 (0.01)	0.46 (0.03)	0.26 (0.01)
	401 (BrC)	0.18	0.29	0.16
	870	0.12 (<0.01)	0.07 (0.01)	0.05 (<0.01)
MSC	401	7.37 (0.06)	5.88 (0.39)	3.65 (0.07)
	530	4.70	3.25	2.41
	870	2.12 (0.02)	1.13 (0.09)	1.14 (0.02)

[a] In this work MAC and MSC values are $PM_{2.5}$ absorption and scattering value divided by $PM_{2.5}$ mass, and values between 401 and 870 nm are obtained from power law fits

[b] In this work MAC and MSC values are $PM_{1.0}$ absorption and scattering value divided by $PM_{2.5}$ mass, and values between 401 and 870 nm are obtained from power law fits.

[c] Values have been adjusted 13% to account for dryer loss in the PAX instrumentation.

These values were lower limits and are not directly comparable to the ones obtained in this study, where the range for both optical and mass measurements goes up to 2.5 µm. Nonetheless, it is useful to list the results from both studies as a range of values, since 1.0 µm cutoffs are common in field campaigns, but $PM_{2.5}$ still remains the default measurement in regional networks. We also note that going to a $PM_{2.5}$ cutoff may have added ash, micro-char and aerosol that is non-combustion generated, such as dust or primary biological aerosol particles, all of which can be physically entrained in wildfire plumes (Formenti et al., 2003; Gaudichet et al., 1995; Hungershoefer et al., 2008).

Several things stand out comparing 2017 and 2018 data in Table 3. The SSA(401) is lower in 2017 (0.93) than 2018 (0.95), but SSA(870) is similar both years consistent with the 2017 smoke being fresher and with higher BrC content. MAC(401) and 870 almost doubled from

2017 to 2018. Since our $\Delta BC/\Delta PM_{2.5}$ also approximately doubled, this makes sense and is not inconsistent with the work of Saleh et al., (2014) who found that the MAC for OA increased with BC/OA (wildfire PM is mostly OA). A contribution to UV absorption from the increased cutoff and thereby sampling more entrained micro-char or dust (Han et al., 2015; Russell et al., 2010) could also play a role. The latter is supported by the ~25% increase in calculated MSC(530). Although the particles in the 1.0-2.5 µm range contribute perhaps 20% of the total particle mass in BB emissions (Reid et al., 2005a), they contributed significantly to both the total absorption and scattering in 2017-18 smoke, but did not strongly affect the SSA.

The SSA is frequently used to calculate aerosol absorption and scattering in models and satellite retrievals. Uncertainty in the SSA is one of the main sources of uncertainty in estimating the radiative effect of aerosols (McComiskey et al., 2008; Jiang and Fiengold, 2006), and assuming constant values of SSA throughout the year may sometimes be inaccurate, as shown by Selimovic et al., (2019) where the SSA at 870 nm in Missoula increased over a month, and Eck et al. (2013), where the SSA at 530 nm in Southern Africa increased by 0.07 between July and October. These increases are consistent with an increase in the smoldering/flaming ratio as regional fuels dry (Akagi et al., 2011; Liu et al., 2014; Pokhrel et al., 2016); Selimovic et al., 2019). Our study average wildfire SSA at 401 nm is slightly higher than the SSA observed in Selimovic et al. (2019), but falls within the observed variability for 870 nm. Our values at both wavelengths are higher than a typical surface SSA of the earth (~0.9, Praveen et al., 2012), which suggests that overall, the wildfire PM measured in this study would contribute to regional cooling (Thornhill et al., 2018; Kolusu et al., 2015). However, Figure 7 shows we do not find an increase in either the SSA at 870 nm or the SSA at 401 nm over the duration of our 2018 sampling period. SSA has been shown to increase as smoke ages (Haywood et al., 2003;

Yokelson et al., 2009; Liu et al., 2014), and the additional aging in the 2018 smoke may have obscured any trend based on flaming or smoldering sources, as we received little impact from local sources in 2018, unlike in 2017 (Selimovic et al., 2019).

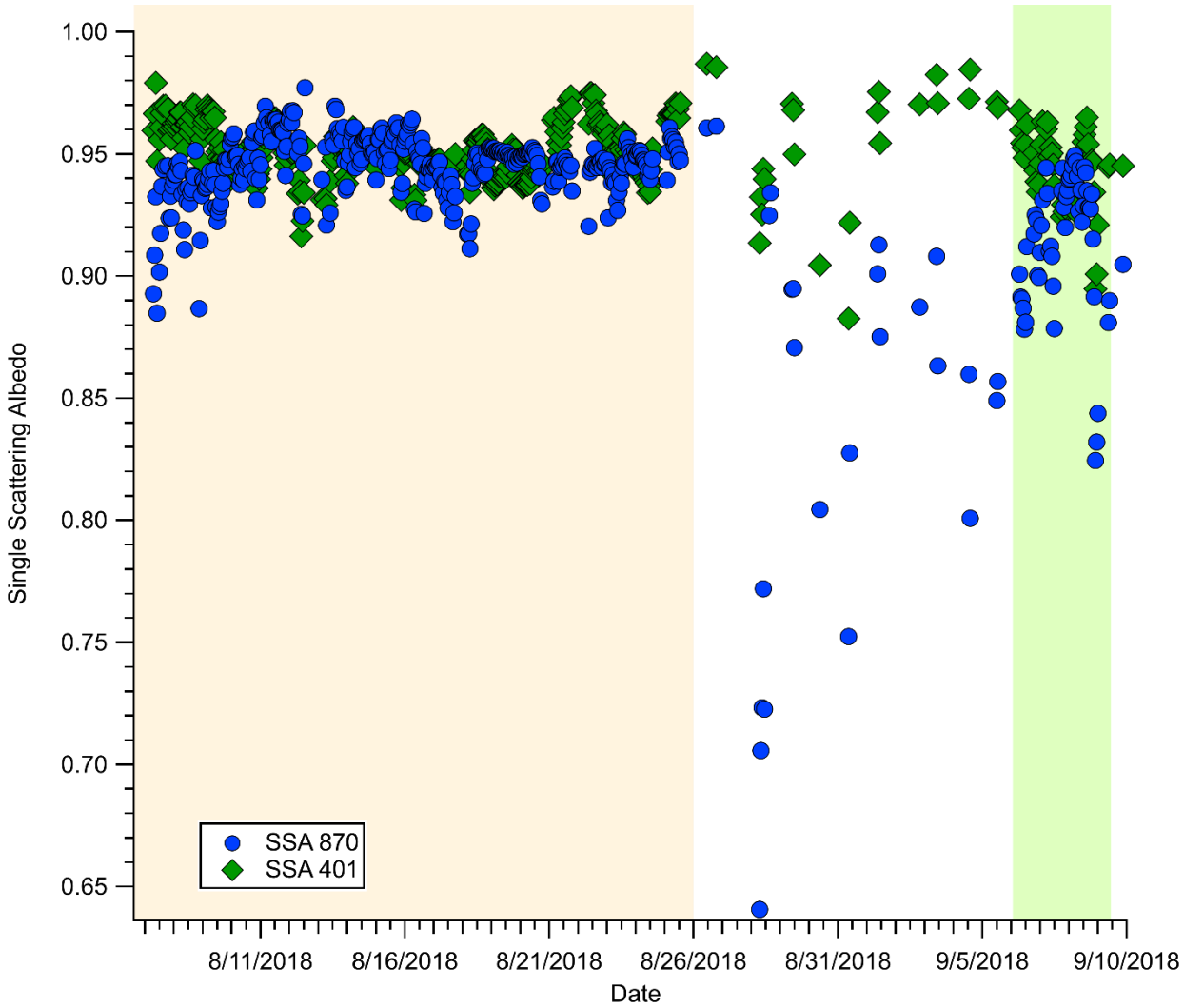

Figure 7. Plot of single scattering albedo at 401 and 870 nm versus the entirety of the sampling duration, calculated for each hour. Sections shaded in yellow represent wildfire smoke impacted periods. Sections shaded in green represent prescribed fire smoke impacted periods. Unshaded areas represent anthropogenic impacts.

5 Conclusions

In this study, we measured smoke properties in 2018 in Missoula, MT, a western urban center that was downwind of numerous wildfires and one prescribed fire. We sampled over 500 h of smoke impacts characterizing CO, aerosol optical properties, effects of wildfire and prescribed fire smoke on O_3 and NO_3 production, and explored how inert tracers and evolving ratios inform

understanding of smoke production and evolution. By comparing and combining with our measurements of less aged smoke in Missoula from 2017 we analyze data for over 1000 h of ambient smoke from western wildfire fuels, primarily coniferous forests. Our low two-year ΔBC/ΔPM average (0.0175 ± 0.0094) confirms the overwhelmingly organic and thus strongly cooling nature of wildfire smoke, and is in line with observations from other field studies. Our 2018 ΔBC/ΔCO ratio (0.0026 ± 0.0007) is almost double the ratio measured in 2017 in Missoula, and suggests a greater influence from lofted smoke produced by flaming combustion, but the average of our ΔBC/ΔCO ratio across two years (0.0020 ± 0.0007) is close to airborne field observations of wildfire smoke. Conversely, ΔPM/ΔCO measured at our surface site across both years was consistently ~50% lower than field studies conducted at higher elevations suggesting that OA evaporation at higher temperatures near the surface may reduce wildfire PM air quality impacts.

On average, O_3 was enhanced when wildfire smoke was present by ~15% (6 ppb) relative to typical clear-sky background levels, with the largest percentage enhancements occurring after sunset and before midnight. The larger O_3 increase after dark likely implies widespread, regionally-enhanced O_3 production upwind, but the arrival of thick smoke just before dark during the prescribed fire impact may have suppressed morning O_3 formation. There appeared to be no smoke impacts on the diurnal cycle of NO_x, suggesting that for the duration of the study, NO_x was likely the result of local emissions. However, NO_3 production rates were elevated relative to background conditions when both wildfire and prescribed fire smoke were present.

On at least one occasion, a nighttime increase in AAE followed, and was likely due to, a spike in $P(NO_3)$. On average, the contribution to absorption at 401 nm by BrC was slightly enhanced at night and loosely followed NO_3 production, but this warrants more study. Despite

the large range in episodic smoke ages across both years, BrC accounted for roughly 50% of the UV-absorption at 401 on average, signifying wide-spread persistence of BrC even as smoke ages and is transported downwind. Obtaining similar AAE values for moderately aged smoke two years in a row implies that our regional smoke AAE value (1.7—2.0) is a useful target for model validation. The SSA at both wavelengths remained consistent over the course of the sampling period, but was higher than the SSA at both wavelengths for anthropogenic aerosol.

Acknowledgments

Vanessa Selimovic and Robert Yokelson were supported by the NSF grants AGS-1748266 and AGS-1349976, NOAA-CPO grant NA16OAR4310100, and NASA grant NNX13AP46G to UM. Gavin McMeeking was supported by the NOAA-CPO grant NA16OAR4310109. Purchase and preparation of the PAXs was supported by NSF grant AGS-1349976 to Robert Yokelson. The authors declare that they have no competing interests. Time series of data used in this paper can be found at https://osf.io/dkjt7/. We would also like to extend our thanks to Ted Christian for maintenance and logistics assistance.

References

Abatzoglou, J. T., & Williams, A. P. (2016), Impact of anthropogenic climate change on wildfire across western US forests, *P. Natl. Acad. Sci. USA*, 113(42), 11770—11775, https://doi.org/10.1073/pnas.1607171113.

Ahern, A. T., Robinson, E. S., Tkacik, D. S., Saleh, R., Hatch, L. E., Barsanti, K. C., Stockwell, C. E., et al. (2019) Production of secondary organic aerosol during aging of biomass-burning smoke from fresh fuels and its relationship to VOC precursors, *J. Geophys. Res.*, 124, 3583–3606 https://doi.org/10.1029/2018JD029068.

Akagi, S. K., Yokelson, R. J., Wiedinmyer, C., Alvarado, M. J., Reid, J. S., Karl, T., Crounse, J. D., & Wennberg, P. O. (2011), Emission factors for open and domestic biomass burning for use in atmospheric models, *Atmos. Chem. Phys.*, 11(9), 4039–4072, doi:10.5194/acp-11-4039-2011.

Akagi, S. K., Craven, J. S., Taylor, J. W., McMeeking, G. R., Yokelson, R. J., Burling I. R., et al. (2012), Evolution of trace gases and particles emitted by a chaparral fire in California, *Atmos. Chem. Phys.*, 12, 1397-1421, https://doi.org/10.5194/acp-12-1397-2012.

Akagi, S. K., Yokelson, R. J., Burling, I. R., Meinardi, S., Simpson, I., Blake, D. R., McMeeking, G. R., et al. (2013), Measurements of reactive trace gases and variable O3 formation rates in some South Carolina biomass burning plumes, *Atmos. Chem. Phys.*, 13(3), 1141–1165, doi:10.5194/acp-13-1141-2013.

Ambrose, J.L., Reidmiller, D.R. & Jaffe, D. A. (2011), Causes of high O3 in the lower free troposphere over the Pacific Northwest as observed at the Mt. Bachelor Observatory. *Atmos. Environ.* 45: 5302–5315, https://doi.org/10.1016/j.atmosenv.2011.06.056.

Benedict, K. B., Prenni, A. J., Carrico, C. M., Sullivan, A. P., Schichtel, B. A., & Collett J. L. Jr. (2017), Enhanced concentrations of reactive nitrogen species in wildfire smoke, *Atmos. Environ.*, 148, 8–15, https://doi.org/10.1016/j.atmosenv.2016.10.030.

Benjamin, S. G., Weygandt, S. S., Brown, J. M., Hu, M., Alexander, C., Smirnova, T. G., et al. (2016), A North American Hourly Assimilation and Model Forecast Cycle: The Rapid Refresh, *Monthly Weather Review*, 144, 1669–1694, https://doi.org/10.1175/MWR-D-15-0242.1.

Bertschi, I.T., Yokelson, R. J., Goode, J. G., Ward, D. E., Babbitt, R.E., Susott, R. A., & Hao, W. M. (2003), Trace gas and particle emissions from fires in large diameter and belowground biomass fuels, *J. Geophys. Res.*, 108, 8472, doi:10.1029/2002JD002100.

Bian, Q., Jathar, S. H., Kodros, J. K., Barsanti, K. C., Hatch, L. E., May, A. A., et al. (2017), Secondary organic aerosol formation in biomass-burning plumes: theoretical analysis of lab studies and ambient plumes, *Atmos. Chem. Phys*., 17, 5459–5475, https://doi.org/10.5194/acp-17-5459-2017.

Birks, J. W., Williford, C. J., Andersen, P. C., Turnipseed, A. A., Strunk, S., & Ennis, C. A. (2018a), Portable ozone calibration source independent of changes in temperature, pressure and humidity for research and regulatory applications, *Atmos. Meas. Tech.*, 11, 4797–4807, https://doi.org/10.5194/amt-11-4797-2018.

Birks, J. W., Andersen, P. C., Williford, C. J., Turnipseed, A. A., Strunk, S. E., Ennis, C. A., & Mattson, E. (2018b), Folded tubular photometer for atmospheric measurements of NO_2 and NO, *Atmos. Meas. Tech.*, 11, 2821–2835, https://doi.org/10.5194/amt-11-2821-2018.

Bond, T. C., Streets, D. G., Yarber, K. F., Nelson, S. M., Woo, J.-H., & Z. Klimont, Z. (2004), A technology-based global inventory of black and organic carbon emissions from combustion, *J. Geophys. Res.*, 109, D14203, doi:10.1029/2003JD003697.

Bond, T. C. & Bergstrom, R. (2006), Light absorption by carbonaceous particles: An investigative review, *Aerosol Sci. Tech.*, 40, 27–67, https://doi.org/10.1080/02786820500421521.

Bond, T. C., Doherty, S. J., Fahey, D.W., Forster, P. M., Berntsen, T., DeAngelo, B. J., et al. (2013), Bounding the role of black carbon in the climate system: A scientific assessment, *J. Geophys. Res.*, 118, 5380-5552, doi:10.1002/jgrd.50171.

Bowman, K. W., Liu, J., Bloom, A. A., Parazoo, N. C., Lee, M., Jiang, Z., Menemenlis, D., (2017), Global and Brazilian Carbon Reponse to El Nino Modoki 2011—2010, *Earth and Space Science*, 4, 637—660, https://doi.org/10.1002/2016EA000204.

Brey, S. J. and Fischer, E. V (2016), Smoke in the City: How Often and Where Does Smoke Impact Summertime Ozone in the United States?, *Environ. Sci. Technol.*, 50, 1288–1294, https://doi.org/10.1021/acs.est.5b05218.

Brown, S. S., Dubé, W. P., Karamchandari, P., Yarwood, G., Peischl, J., Ryerson, T. B., et al. (2012), The effects of NOx control and plume mixing on nighttime chemical processing of plumes from coal-fired power plants, *J. Geophys. Res.*, 117, D07304, doi:10.1029/2011JD016954.

Brown, S. S., Dubé, W. P., Bahreini, R., Middlebrook, A. M., Brock, C. A., Warneke, C., et al. (2013), Biogenic VOC oxidation and organic aerosol formation in an urban nocturnal boundary layer: Aircraft vertical profiles in Houston, TX. *Atmos. Chem. Phys.*, 13, 11317-11337.

Burkholder, J. B., Sander, S. P., Abbatt, J., Barker, J. R., Huie, R. E., Kolb, C. E., Kurylo, M. J., (2015), "Chemical Kinetics and Photochemical Data for Use in Atmospheric Studies, Evaluation No. 18", *JPL Publication* 15-10, Jet Propulsion Laboratory, Pasadena, http://jpldataeval.jpl.nasa.gov.

Burling, I. R., Yokelson, R. J., Akagi, S. K., Urbanski, S. P., Wold, C. E., Griffith, D. W. T., et al. (2011), Airborne and ground-based measurements of the trace gases and particles emitted by prescribed fires in the United States, *Atmos. Chem. Phys.*, 11, 12197–12216, doi:10.5194/acp-11-12197-2011.

Campbell, J., Donato, D., Azuma, D., & Law, B. (2007), Pyrogenic carbon emission from a large wildfire in Oregon, United States, *J. Geophys. Res*., 112, G04014, doi:10.1029/2007JG000451.

Capes, G., Johnson, B., McFiggans, G., Williams, P. I., Haywood, J., & Coe, H. (2008), Aging of biomass burning aerosols over West Africa: Aircraft measurements of chemical composition, microphysical properties, and emission ratios, *J. Geophys. Res*., 113, D00C15, doi:10.1029/2008JD009845.

Chen, J., Li, C., Ritovski, Z., Milic, A., Gu, Y., Islam, M., et al. (2017), A review of biomass burning: Emissions and impacts on air quality, health, and climate in China, *Sci. Total Environ*., 579, 1000—1034, https://doi.org/10.1016/j.scitotenv.2016.11.025.

Clarke, A. D., Shinozuka, Y., Kapustin, V. N., Howell, S., Huebert, B., Doherty, S., et al. (2004), Size distributions and mixtures of dust and black carbon aerosol in Asian outflow: Physiochemistry and optical properties, *J. Geophys. Res*., 109, D15S09, doi:10.1029/2003jd004378.

Collier, S., Zhou, S., Onasch, T.B., Jaffe, D. A., Kleinman, L., Sedlacek, A. J. III., et al. (2016), Regional influence of aerosol emissions from wildfires driven by combustion efficiency: insights from the BBOP campaign, *Environ. Sci. Technol*., 50(16), 8513-22, doi:10.1021/acs.est.6b01617.

Crutzen, P. J. & Andreae, M. O. (1990), Biomass burning in the tropics: Impact on atmospheric chemistry and biogeochemical cycles, *Science*, 250, 1669–1678, doi:10.1126/science.250.4988.1669.

Cubison, M. J., Ortega, A. M., Hayes, P. L., Farmer, D. K., Day, D., Lechner, M. J., et al. (2011), Effects of aging on organic aerosol from open biomass burning smoke in aircraft and laboratory studies, *Atmos. Chem. Phys*., 11, 12049–12064, https://doi.org/10.5194/acp-11-12049-2011.

Decker, Z. C. J., Zarzana, K. J., Coggon, M., Min, K. E., Pollack, I., Ryerson, T. B., et al. (2019), Nighttime Chemical Transformation in Biomass Burning Plumes: A Box Model Analysis Initialized with Aircraft Observations, *Environ. Sci. Technol*., 53(5), 2529—2538, doi: 10.1021/acs.est.8b05359.

Doerr, S. H., & Santin, C. (2016), Global trends in wildfire and its impacts: perceptions versus realities in a changing world, *Philos. T. Roy. Soc. B*., 371(1696), https://doi.org/10.1098/rstb.2015.0345.

Draxler, R.R., & Hess, G. D. (1997), Description of the HYSPLIT_4 modeling system. NOAA Tech. Memo. ERL ARL-224, NOAA Air Resources Laboratory, Silver Spring, MD, 24 pp.

Draxler, R.R., & Hess, G. D. (1998), An overview of the HYSPLIT_4 modeling system of trajectories, dispersion, and deposition. *Aust. Meteor. Mag.*, 47, 295-308.

Draxler, R.R. (1999), HYSPLIT4 user's guide. NOAA Tech. Memo. ERL ARL-230, NOAA Air Resources Laboratory, Silver Spring, MD.

Ervens, B., Turpin, B. J., & Weber, R.J. (2011), Secondary organic aerosol formation in cloud droplets and aqueous particles (aqSOA): a review of laboratory, field and model studies, *Atmos. Chem. Phys.*, 11, 11069-11102, https://doi.org/10.5194/acp-11-11069-2011.

Feng, Y., Ramanathan, V., & Kotamarthi, V. R. (2013), Brown carbon: a significant atmospheric absorber of solar radiation?, *Atmos. Chem. Phys.*, 13, 8607–8621, doi:10.5194/acp-13-8607-2013.

Fleming, L. T., Lin, P., Roberts, J. M., Selimovic, V., Yokelson, R., Laskin, J., et al. (2019), Molecular composition and photochemical lifetimes of brown carbon chromophores in biomass burning organic aerosol, *Atmos. Chem. Phys. Discuss*., https://doi.org/10.5194/acp-2019-523.

Formenti, P., Elbert, W., Maenhaut, W., Haywood, J., Osborne, S., & Andreae, M. O. (2003), Inorganic and carbonaceous aerosols during the Southern African Regional Science Initiative (SAFARI 2000) experiment: Chemical characteristics, physical properties, and emission data for smoke from African biomass burning, *J. Geophys. Res*., 108, 8488, https://doi.org/10.1029/2002JD002408.

Forrister, H., Liu, J., Scheuer, E., Dibb, J., Ziemba, L., Thornhill, K. L., et al. (2015), Evolution of brown carbon in wildfire plumes. *Geophys. Res. Lett*., 42, 4623-4630, doi:10.1002/2015GL063897.

Fromm, M., Alfred, J., Hoppel, K., Hornstein, J., Bevuilacqua, R., Shettle, E., et al. (2000), Observations of boreal forest fire smoke in the stratosphere by POAM III, SAGE II, and lidar in 1998, *J. Geophys. Res*., 27(9), 1407—1410, https://doi.org/10.1029/1999GL011200.

Garofalo, L. A., Pothier, M. A., Levin, E. J. T., Campos, T. Kreidenweis, S. M., & Farmer, D. K. (2019), Emission and Evolution of Submicron Organic Aerosol in Smoke from Wildfires in the Western United States, *ACS Earth Space Chem*., 3, 1237—1247.

Gaudichet, A., Echalar, F., Chatenet, B. Quisefit, J. P., Malingre, G., Cachier, H., et al. (1995), Trace elements in tropical African savanna biomass burning aerosols, *J. Atmos. Chem*., 22(1-2), 19—39, doi:10.1007/BF00708179.

Gilman, J. B., Lerner, B. M., Kuster, W. C., Goldan, P. D., Warneke, C., Veres, P. R.,et al. (2015), Biomass burning emissions and potential air quality impacts of volatile organic compounds and other trace gases from fuels common in the US, *Atmos. Chem. Phys*., 15, 13915-13938, doi:10.5194/acp-15-13915-2015.

Graber, E. R. & Rudich, Y. (2006), Atmospheric HULIS: How humic-like are they? A comprehensive and critical review, *Atmos. Chem. Phys*., 6, 729-753, https://doi.org/10.5194/acp-6-729-2006.

Griffith, D. W. T., (1996), Synthetic calibration and quantitative analysis of gas phase infrared spectra, *Appl. Spectrosc*., 50, 59–70.

Hardy, C. C., Regelbrugge, J. C., & Teesdale, D. R. (1996) Smoke emissions from prescribed burning of southern California chaparral, Res. Pap. PNW-RP-486, US Department of Agriculture, Forest Service, Pacific Northwest Research Station, Portland, OR. https://doi.org/10.2737/PNW-RP-486.

Han, Y., Wu, Y., Wang, T., Xie, C., Zhao, K., Zhuang, B., & Li, S. (2015), Characterizing a persistent Asian dust transport event: Optical properties and impact on air quality through the ground-based and satellite measurements over Nanjing, China, *Atmos. Environ*. 115, 304—316, https://doi.org/10.1016/j.atmosenv.2015.05.048, 2015.

Hammer, M. S., Martin, R. V., van Donkelaar, A., Buchard, V., Torres, O., Ridley, D. A., & Spurr, R. J. D. (2016), Interpreting the ultraviolet aerosol index observed with the OMI satellite instrument to understand absorption by organic aerosols: implications for atmospheric oxidation and direct radiative effects, *Atmos. Chem. Phys*., 16, 2507–2523, https://doi.org/10.5194/acp16-2507-2016.

Hatch, L. E., Yokelson, R. J., Stockwell, C. E., Veres, P. R., Simpson, I. J., Blake, D. R., Orlando, J. J., & Barsanti, K. C. (2017) Multi-instrument comparison and compilation of non-methane organic gas emissions from biomass burning and implications for smoke-derived secondary organic aerosol precursors, *Atmos. Chem. Phys.*, 17, 1471–1489, https://doi.org/10.5194/acp-17-1471-2017.

Hatch, L. E., Rivas-Ubach, A., Jen, C. N., Lipton, M., Goldstein, A. H., & Barsanti, K. C. (2018) Measurements of I/SVOCs in biomass-burning smoke using solid-phase extraction disks and two-dimensional gas chromatography, *Atmos. Chem. Phys*., 18, 17801–17817, https://doi.org/10.5194/acp-18-17801-2018.

Haywood, J. M., Osborne, S. R., Francis, P. N., Keil, A., Formenti, P., Andreae, M. O., & Kaye, P. H. (2003) The mean physical and optical properties of regional haze dominated by biomass burning aerosol measured from the C-130 aircraft during SAFARI 2000, *J. Geophys. Res.*, 108(D13), https://doi.org/10.1029/2002JD002226.

Hecobian, A., Zhang, X., Zheng, M., Frank, N., Edgerton, E. S., & Weber, R. J. (2010), Water-Soluble Organic Aerosol material and the light-absorption characteristics of aqueous extracts measured over the Southeastern United States, *Atmos. Chem. Phys*., 10, 5965-5977, https://doi.org/10.5194/acp-10-5965-2010.

Herron-Thorpe, F. L., Mount, G. H., Emmons, L. K., Lamb, B. K., Jaffe, D. A., Wigder, N. L., et al. (2014), Air quality simulations of wildfires in the Pacific Northwest evaluated with surface and satellite observations during the summers of 2007 and 2008, *Atmos. Chem. Phys*., 14, 12533-12551, doi:10.5194/acp-14-12533-2014.

Hungershoefer, K., Zeromskiene, K., Iinuma, Y., Helas, G., Trentmann, J., Trautmann, T., et al. (2008), Modeling the optical properties of fresh biomass burning aerosol produced in a

smoke chamber: results from the EFEU campaign, *Atmos. Chem. Phys*., 8, 3427-3439, https://doi.org/10.5194/acp-8-3427-2008.

Iinuma, Y., Böge, O., Gräfe, R., & Herrmann, H. (2010), Methylnitrocatechols: atmospheric tracer compounds for biomass burning secondary organic aerosols, *Environ. Sci. Technol*., 44, 8453e8459, https://doi.org/10.1021/es102938a.

Jacob, D. J., Crawford, J. H., Maring, H., Clarke, A. D., Dibb, J. E., Emmons, L. K., et al. (2010), The Arctic Research of the Composition of the Troposphere from Aircraft and Satellites (ARCTAS) mission: design, execution, and first results, *Atmos. Chem. Phys.*, 10, 5191-5212, https://doi.org/10.5194/acp-10-5191-2010.

Jacobson, M. Z. (2014), Effects of biomass burning on climate, accounting for heat and moisture fluxes, black and brown carbon, and cloud absorption effects, *J. Geophys. Res. Atmos*., 119, 8980-9002, doi:10.1002/2015JD021861.

Jaffe, D. A., Wigder, N., Downey, N., Pfister, G., Boynard, A., & Reid, S. B. (2013) Impact of wildfires on ozone exceptional events in the western U.S., *Environ. Sci. Technol*., 47(19), 11065—11072, doi:10.1021/es402164f.

Jaffe, D. A., Cooper, O. R., Fiore, A. M., Henderson, B. H., Gail, S., Russell, A. G., et al. (2018), Scientific assessment of background ozone over the U.S.: implications for air quality management, *Elem. Sci. Anthr*., 6, 56, https://doi.org/10.1525/elementa.309.

Jen, C. N., Hatch, L. E., Selimovic, V., Yokelson, R. J., Weber, R., Fernandez, A. E., Kreisberg, N. M., et al. (2019), Speciated and total emission factors of particulate organics from burning western US wildland fuels and their dependence on combustion efficiency, *Atmos. Chem. Phys.*, 19, 1013-1026, https://doi.org/10.5194/acp-19-1013-2019.

Jethva, H. & Torres, O. (2011), Satellite-based evidence of wavelength-dependent aerosol absorption in biomass burning smoke inferred from Ozone Monitoring Instrument, *Atmos. Chem. Phys.*, 11, 10541-10551, https://doi.org/10.5194/acp-11-10541-2011.

Jiang, H., & Feingold, G. (2006), Effect of aerosol on warm convective clouds: aerosol-cloud-surface flux feedbacks in a new coupled large eddy model, *J. Geophys. Res. Atmos*., 111(D1), https://doi.org/10.1029/2005JD006138.

Jolly, W. M., Cochrane, M. A., Freeborn, P. H., Holden, Z. A., Brown, T. J., Williamson, G. J., & Bowman, D. M. J. S. (2015), Climate-induced variations in global wildfire danger from 1979 to 2013, *Nat. Commun*., 6, 7537, doi:10.1038/ncomms8537.

Kolusu, S. R., Marsham, J. H., Mulcahy, J., Johnson, B., Dunning, C., Bush, M., & Spracklen, D. V. (2015), Impacts of Amazonia biomass burning aerosols assessed from short-range weather forecasts, *Atmos. Chem. Phys*., 15, 12251-12266, https://doi.org/10.5194/acp-15-12251-2015.

Koss, A. R., Sekimoto, K., Gilman, J. B., Selimovic, V., Coggon, M. M., Zarzana, K. J., et al. (2018), Non-methane organic gas emissions from biomass burning: identification,

quantification, and emission factors from PTR-ToF during the FIREX 2016 laboratory experiment, *Atmos. Chem. Phys*., 18, 3299-3319, https://doi.org/10.5194/acp-18-3299-2018.

Lack, D. A., Cappa, C. D., Covert, D. S., Baynard, T., Massoli, P., Sierau, B., et al. (2008), Bias in Filter Based Aerosol Light Absorption Measurements Due to Organic Aerosol Loading: Evidence from Ambient Measurements, *Aerosol Sci. Tech*., 42, 1033–1041, https://doi.org/10.1080/02786820802389285.

Lack, D. A. & Cappa, C D. (2010), Impact of brown and clear carbon on light absorption enhancement, single scatter albedo and absorption wavelength dependence of black carbon, *Atmos. Chem. Phys*., 10, 4207-4220, https://doi.org/10.5194/acp-10-4207-2010.

Lack, D. A. & Langridge, J. M. (2013), On the attribution of black and brown carbon light absorption using the Ångström exponent, *Atmos. Chem. Phys*., 13, 10535-10543, https://doi.org/10.5194/acp-13-10535-2013.

Laskin, A., Laskin, J., & Nizkorodov, S. A. (2015), Chemistry of atmospheric brown carbon, *Chem. Rev*., 115(10), 4335-4382, doi:10.1021/cr5006167.

Lewis, K., Arnott, W. P., Moosmuller, H., & Wold, C. E. (2008), Strong spectral variation of biomass smoke light absorption and single scattering albedo observed with a novel dual-wavelength photoacoustic instrument, *J. Geophys. Res*., 113, D16203, doi:10.1029/2007JD009699.

Lee, J. D., Moller, S. J., Read, K. A., Lewis, A. C., Mendes, L., & Carpenter, L. J. (2009), Year-round measurements of nitrogen oxides and ozone in the tropical North Atlantic marine boundary layer, *J. Geophys. Res*., 114, D21302, doi:10.1029/2009JD011878.

Li, Y. & Shiraiwa, M. (2019), Timescales of secondary organic aerosols to reach equilibrium at various temperatures and relative humidities, *Atmos. Chem. Phys*., 19, 5959–5971, https://doi.org/10.5194/acp-19-5959-2019.

Lim, C. Y., Hagan, D. H., Coggon, M. M., Koss, A. R., Sekimoto, K., de Gouw, J., et al. (2019), Secondary organic aerosol formation from the laboratory oxidation of biomass burning emissions, *Atmos. Chem. Phys*., 19, 12797–12809, https://doi.org/10.5194/acp-19-12797-2019.

Lindaas, J., Farmer, D. K., Pollack, I. B., Abeleira, A., Flocke, F., Roscioli, R., Herndon, S., & Fischer, E. V. (2017), Changes in ozone and precursors during two aged wildfire smoke events in the Colorado Front Range in summer 2015, *Atmos. Chem. Phys*., 17, 10691-10707, https://doi.org/10.5194/acp-17-10691-2017.

Liu J., Scheuer, E., Dibb, J., Ziemba, L. D., Thornhill, K. L., Anderson, B. E. et al. (2014), Brown carbon in the continental troposphere, *Geophys. Res. Lett*., 41(6), 2191—2195, https://doi.org/10.1002/2013GL058976.

Liu, X., Zhang, Y., Huey, L. G., Yokelson, R. J., Wang, Y., Jimenez, J. L., et al. (2016), Agricultural fires in the southeastern U.S. during SEAC^{4}RS: Emissions of trace gases and particles and evolution of ozone, reactive nitrogen, and organic aerosol, *J. Geophys. Res. Atmos*., 121, 7383—7414, https://doi.org/10.1002/2016JD025040.

Liu, X., Huey, G. L., Yokelson, R. J., Selimovic, V., Simpson, I. J., Müller, M., et al. (2017), Airborne measurements of western U.S wildfire emissions: Comparison with prescribed burning and air quality implications, *J. Geophys. Res. Atmos*., 122, 6108-6129, doi:10.1002/2016JD026315.

Liu, C., Chung, C. E., Yin, Y., & Schnaiter, M. (2018), The absorption Ångström exponent of black carbon: from numerical aspects, *Atmos. Chem. Phys*., 18, 6259–6273, https://doi.org/10.5194/acp-18-6259-2018.

Marlon, J. R., Bartlein, P. J., Gavin, D. G., Long, C. J., Anderson, R. S., Briles, C. E., et al. (2012) Long-term perspective on wildfires in the western USA, *P. Natl. Acad. Sci. USA*, 109(9), E535—E543, https://doi.org/10.1073/pnas.1112839109.

May, A. A., Levin, E. J. T., Hennigan, C. J., Riipinen, I., Lee, T., Collett J. L. Jr. et al. (2013), Gas-particle partitioning of primary organic aerosol emissions: 3. Biomass burning, *J. Geophys. Res. Atmos*., 118, 11,327–11,338, doi:10.1002/jgrd.50828.

May, A. A., McMeeking., G. R., Lee, T., Taylor, J. W., Craven, J. S., Burling, I., et al. (2014), Aerosol emissions from prescribed fires in the United States: A synthesis of laboratory and aircraft measurements, *J. Geophys. Res. Atmos*., 119, 11826-11849, doi:10.1002/2014JD021848.

May, A. A., Lee, T., McMeeking, G. R., Akagi, S., Sullivan, A. P., Urbanski, S., et al. (2015), Observations and analysis of organic aerosol evolution in some prescribed fire smoke plumes, *Atmos. Chem. Phys*., 15, 6323–6335, https://doi.org/10.5194/acp-15-6323-2015.

McComiskey, A., Schwartz, S. E., Schmid, B., Guan, H., Lewis, E. R., Ricchiazzi, P., & Ogren, J. A. (2008), Direct aerosol forcing: calculation from observables and sensitivities to inputs, *J. Geophys. Res. Atmos*., 113(D9), https://doi.org/10.1029.2007JD009170.

Miyakawa, T., Oshima, N., Taketani, F., Komazaki, Y., Yoshino, A., Takami, A., et al. (2017), Alteration of the size distributions and mixing states of black carbon through transport in the boundary layer in east Asia, *Atmos. Chem. Phys*., 17, 5851-5864, https://doi.org/10.5194/acp-17-5851-2017.

Mohr, C., Lopez-Hilfiker, F., Zotter, P., Prévôt, A. S. H., Xu, L., Ng, N. L., et al. (2013), Contribution of nitrated phenols to wood burning brown carbon light absorption in Detling, United Kingdom during winter time, *Environ. Sci. Technol*., 47, 6316–6324, https://doi.org/10.1021/es400683v.

Morgan, W. T., Allan, J. D., Bauguitte, S., Darbyshire, E., Flynn, M. J., Lee, J., et al. (2019), Transformation and aging of biomass burning carbonaceous aerosol over tropical South

America from aircraft in-situ measurements during SAMBBA, *Atmos. Chem. Phys. Discuss*., https://doi.org/10.5194/acp-2019-157.

Morris, G. A., Hersey, S., Thompson, A. M., Paweson, S., Nielsen, J. E., Colarco, P. R., et al. (2006), Alaskan and Canadian forest fires exacerbate ozone pollution over Houston, Texas, on 19 and 20 July 2004, *J. Geophys. Res*., 111, D24S03, doi:10.1029/2006JD007090.

Nakayama, T. Suzuki, H., Kagamitani, S., & Ikeda, Y. (2015), Characterization of a three wavelength Photoacoustic Soot Spectrometer (PASS-3) and a Photoacoustic Extinctiometer (PAX), *J. Meteorol. Soc. Japan*, 93(2), 285–308, doi:10.2151/jmsj.2015-016.

Nergui, T., Lee, Y., Chung, S. H., Lamb, B. K., Yokelson, R. J., & Barsanti, K.(2017), Integrating Measurement Based New Knowledge on Wildland Fire Emissions and Chemistry into the AIRPACT Air Quality Forecasting for the Pacific Northwest, American Geophysical Union Fall Meeting, New Orleans, LA, Abstract# A41L-06.

Palm, B. B., Campuzano-Jost, P., Day, D. A., Ortega, A. M., Fry, J. L., Brown, S. S., et al. (2017) Secondary organic aerosol formation from in situ OH, O_3, and NO_3 oxidation of ambient forest air in an oxidation flow reactor, *Atmos. Chem. Phys*., 17, 5331–5354, https://doi.org/10.5194/acp-17-5331-2017.

Peterson, D., Fromm, M. D., Solbrig, J. E., Hyer, E. J., Surratt, M. L., & Campbell, J. R. (2017), Detection and Inventory of Intense Pyroconvection in Western North America using *GOES-1*5 Daytime Infrared Data, *American Meteorological Society*, https://doi.org/10.1175/JAMC-D-16-0226.1.

Pokhrel, R. P., Wagner, N. L., Langridge, J. M., Lack, D. A., Jayarathne, T., et al. (2016), Parameterization of single-scattering albedo (SSA) and absorption Ångström exponent (AAE) with EC / OC for aerosol emissions from biomass burning, *Atmos. Chem. Phys*., 16, 9549-9561, https://doi.org/10.5194/acp-16-9549-2016.

Pokhrel, R. P., Beamesderfer, E. R., Wagner, N. L., Langridge, J. M., Lack, D. A., Jayarathne, T., et al. (2017), Relative importance of black carbon, brown carbon, and absorption enhancement from clear coatings in biomass burning emissions, *Atmos. Chem. Phys*., 17, 5063-5078, https://doi.org/10.5194/acp-17-5063-2017.

Praveen, P. S., Ahmed, T., Kar, A., Rehman, I. H., & Ramanathan, V. (2012), Link between local scale BC emissions and large scale atmospheric solar absorption, *Atmos. Chem. Phys*., 12, 1173–1187, doi:10.5194/acp-12-1173-2012.

Reid, J. S., Koppmann, R., Eck, T. F., & Eleuterio, D. P. (2005a), A review of biomass burning emissions part II: intensive physical properties of biomass burning particles, *Atmos. Chem. Phys.*, 5, 799– 825, doi:10.5194/acp-5-799-2005.

Reid, J. S., Eck, T. F., Christopher, S. A., Koppmann, R., Dubovik, O., Eleuterio, D. P., et al. (2005b) A review of biomass burning emissions part III: intensive optical properties of

biomass burning particles, *Atmos. Chem. Phys*., 5, 827-849, https://doi.org/10.5194/acp-5-827-2005.

Robinson, A. L., Donahue, N. M., Shirvastava, M. K, Weitkamp, E. A., Sage, A. M., Grieshop, A. P., et al. (2007), Rethinking organic aerosols: Semivolatile emissions and photochemical aging, *Science*, 315(5816), 1259—1262, doi:10.1126/science.1133061.

Rothman, L. S., Gordon, I. E., Barbe, A., Benner, D. C., Bernath, P. F., Birk, M., et al. (2009), The HITRAN 2008 molecular spectroscopic database, *J Quant. Spectrosc. Ra*., 110(9-10), 533—572.

Russell, P. B., Bergstrom, R. W., Shinozuka, Y., Clarke, A. D., DeCarlo, P. F., Jimenez, J. L., et al. (2010), Absorption Angstrom Exponent in AERONET and related data as an indicator of aerosol composition, *Atmos. Chem. Phys*., 10, 1155-1169, https://doi.org/10.5194/acp-10-1155-2010, 2010.

Sahu, L. K., Kondo, Y., Moteki, N., Takegawa, N., Zhao, Y., Cubison, M. J., et al. (2012), Emission characteristics of black carbon in anthropogenic and biomass burning plumes over California during ARCTAS-CARB 2008, *J. Geophys. Res-Atmos*, 117(D16), doi:10.1029/2011JD017401.

Saide, P. E., Peterson, D. A., da Silva, A., Anderson, B., Ziemba, L. D., Diskin, G., et al. (2015), Revealing important nocturnal and day-to-day variations in fire smoke emissions through a multiplatform inversion, *Geophys. Res. Lett*., 42(9), 2015GL063737, doi:10.1002/2015GL063737.

Saleh, R., Robinson E. S., Tkacik, D. S., Ahern, A. T., Liu, S., Aiken, A. C., et al. (2014), Brownness of organics in aerosols from biomass burning linked to their black carbon content. *Nature Geoscience*, 7, 647-650, doi:10.1038/ngeo2220.

Santin, C., Doerr, S. H., Preston, C. M., & Gonzalez-Rodriguez, G (2015), Pyrogenic organic matter production from wildfires: a missing sink in the global carbon cycle, *Glob. Chang Biol*., 21(4), 1621—1633, https://doi.org/10.1111/gcb.12800.

Schoennagel, T., Balch, J. K., Brenkert-Smith, H., Dennison, P. E., Harvey, B. J., Krawchuk, M. A., et al. (2017), Adapt to more wildfire in western North American forests as climate changes, *P. Natl. Acad. Sci. USA*., 114(18), 4582—4590, https://doi.org/10.1073/pnas.1617464114.

Sedlacek III, A. J., Buseck, P. R., Adachi, K., Onasch, T. B., Springston, S. R., & Kleinman, L. (2018), Formation and evolution of tar balls from northwestern US wildfires, *Atmos. Chem. Phys*., 18, 11289–11301, https://doi.org/10.5194/acp-18-11289-2018.

Selimovic, V., Yokelson, R. J., Warneke, C., Roberts, J. M., de Gouw, J., Reardon, J., & Griffith, D. W. T (2018), Aerosol optical properties and trace gas emissions by PAX and OP-FTIR for laboratory-simulated western US wildfires during FIREX, *Atmos. Chem. Phys*., 18, 2929-2948, https://doi.org/10.5194/acp-18-2929-2018.

Selimovic, V., Yokelson, R. J., McMeeking, G. R., & Coefield, S. (2019), In situ measurements of trace gases, PM, and aerosol optical properties during the 2017 NW US wildfire smoke event, *Atmos. Chem. Phys.*, 19, 3905–3926, https://doi.org/10.5194/acp-19-3905-2019.

Selimovic, V. (2019), MSO Smoke Monitoring (V1). Retrieved from DOI 10.17605/OSF.IO/DKJT7.

Shaddix, C. R., Harrington, J. E., & Smyth, K. C (1994), Quantitative measurements of enhanced soot production in a flickering methane/air diffusion flame, *Combust. Flame.*, 99(3-4), 723-732, https://doi.org/10.1016/0010-2180(94)90067-1.

Shivdenko, A. Z., & Schepaschenko, D. G (2013), Climate change and wildfires in Russia, *Contemp. Probl. Eco.*, 6(7), 683—692, doi: https://doi.org/10.1134/S199542551307010X.

Stocks, B. J., van Wilgen, B. W., Trollope, W. S. W., McRae, D. J., Mason, J. A., Weirich, F., & Potgieter, A. L. F. (1996), Fuels and fire behavior dynamics on large-scale savanna fires in Kruger National Park, South Africa, *J. Geophys. Res. Atmos.*, 101(D19), 23541—23550.

Stein, A.F., Draxler, R.R, Rolph, G.D., Stunder, B.J.B., Cohen, M.D., & Ngan, F. (2015), NOAA's HYSPLIT atmospheric transport and dispersion modeling system, *Bull. Amer. Meteor. Soc*., 96, 2059-2077, http://dx.doi.org/10.1175/BAMS-D-14-00110.1.

Stevens, J. T., Safford, H. G., & Latimer, A. M (2014), Wildfire-contigent effects of fuel treatments can promote ecological resilience in seasonally dry conifer forests, *Can. J. Forest Res*., 44(5), 843—854, https://doi.org/10.1139/cjfr-2013-0460.

Stockwell, C. E., Veres, P. R., Williams, J., & Yokelson, R. J. (2015), Characterization of biomass burning emissions from cooking fires, peat, crop residue, and other fuels with high-resolution proton-transfer-reaction time-of-flight mass spectrometry, *Atmos. Chem. Phys*., 15, 845-865, https://doi.org/10.5194/acp-15-845-2015.

Stockwell, C. E., Jayarathne, T., Cochrane, M. A., Ryan, K. C., Putra, E. I., Saharjo, B. H., et al. (2016a), Field measurements of trace gases and aerosols emitted by peat fires in Central Kalimantan, Indonesia, during the 2015 El Niño, *Atmos. Chem. Phys*., 16, 11711-11732, https://doi.org/10.5194/acp-16-11711-2016.

Stockwell, C. E., Christian, T. J., Goetz, J. D., Jayarathne, T., Bhave, P. V., Praveen, P. S., et al. (2016b), Nepal Ambient Monitoring and Source Testing Experiment (NAMaSTE): emissions of trace gases and light-absorbing carbon from wood and dung cooking fires, garbage and crop residue burning, brick kilns, and other sources, Atmos. Chem. Phys., 16, 11043-11081, https://doi.org/10.5194/acp-16-11043-2016.

Subramanian, R., Roden, C. A., Boparai, P., & Bond, T. C (2007), Yellow beads and missing particles: trouble ahead for filter-based absorption measurements, *Aerosol. Sci. Tech*., 41(6), 630-637, https://doi.org/10.1080/02786820701344589.

Thornhill, G. D., Ryder, C. L., Highwood, E. J., Shaffrey, L. C., & Johnson, B. T. (2018), The effect of South American biomass burning aerosol emissions on the regional climate, *Atmos. Chem. Phys*., 18, 5321-5342, https://doi.org/10.5194/acp-18-5321-2018.

Tkacik, D. S., Robinson, E. S., Ahern, A., Saleh, R., Stockwell, C., Simpson, I. J., et al. (2017), A dual-chamber enhancement method for quantifying effects of atmospheric perturbations on secondary organic aerosol formation from biomass burning emissions, *J. Geophys. Res. Atmos.*, 122, doi:10.1002/2016JD025784.

Tomaz, S, Cui, T., Chen, Y., Sexton, K. G., Roberts, J. M., Warneke, C., et al. (2018), Photochemical cloud processing of primary wildfire emissions as a potential source of secondary organic aerosol, *Environ. Sci. Technol*., 52(19), 11027—11037, doi:10.1021/acs.est.8b03293.

Turner, M. G., Braziunas, K. H., Hansen, W. D., & Harvey, B. J (2019), Short-interval severe fire erodes the resilience of subalpine Lodgepole pine forest, *P. Natl. Acad. Sci. USA*, 116 (23), 11319—11328, doi:10.1073/pnas.1902841116.

United States Department of Agriculture (2015), The Rising Cost of Wildfire Operations: Effects on the Forest Service's Non-Fire Work, https://www.fs.fed.us/sites/default/files/2015-Fire-Budget-Report.pdf.

Vakkari, V., Beukes, J. P., Dal Maso, M., Aurela, M., Josipovic, M. & van Zyl, P. G. (2018), Major secondary aerosol formation in southern African open biomass burning plumes, *Nature Geosci*., 11, 580–583, doi:10.1038/s41561-018-0170-0.

Wagenbrenner, N. S., Forthofer, J. M., Lamb, B. K., Shannon, K. S., & Butler, B. W. (2016), Downscaling surface wind predictions from numerical weather prediction models in complex terrain with WindNinja, *Atmos. Chem. Phys*., 16, 5229–5241, https://doi.org/10.5194/acp-16-5229-2016.

Wang, J., Geng, N. B., Xu, Y. F., Zhang, W. D., Tang, X. Y., & Zhang, R. Q. (2014), PAHs in PM2.5 in Zhengzhou: concentration, carcinogenic risk analysis and source apportionment, *Environ. Monit. Assess*., 186(11), 7461-7473, https://doi.org/10.1007/s10661-014-3940-1.

Wang, J., Yue, Y., Wang, Y., Ichoku, C., Ellison, L., & Zeng, J. (2017) Mitigating satellite-bassed fire sampling limitations in deriving biomass burning emission rates: application to WRF-Chem model over the northern sub-saharan African region, *J. Geophys. Res.-Atmos*, 123(1), 507-528, https://doi.org/10.1002/2017JD026840.

Westerling, A. L., Hidalgo, H. G., Cayan, D. R., & Swetnam, T. W. (2006), Warming and earlier spring increase western U.S forest wildfire activity, *Science*, 313 (5789), 940-943, doi:10.1126/science.1128834.

Yokelson, R.J., T.J. Christian, I.T. Bertschi, & W.M. Hao (2003), Evaluation of adsorption effects on measurements of ammonia, acetic acid, and methanol, J. Geophys. Res. 108, 4649, doi:10.1029/2003JD003549.

Yokelson, R. J., Karl, T., Artaxo, P., Blake, D. R., Christian, T. J., Griffith, D. W. T., et al. (2007) The Tropical Forest and Fire Emissions Experiment: overview and airborne fire emission factor measurements, *Atmos. Chem. Phys*., 7, 5175–5196, doi:10.5194/acp-7-5175-2007.

Yokelson, R. J., Christian, T. J., Karl, T. G., & Guenther, A. (2008), The tropical forest and fire emissions experiment: laboratory fire measurements and synthesis of campaign data, *Atmos. Chem. Phys*., 8, 3509-3527, doi:10.5194/acp-8-3509-2008.

Yokelson, R. J., Crounse, J. D., DeCarlo, P. F., Karl, T., Urbanski, S., Atlas, E., et al. (2009), Emissions from biomass burning in the Yucatan, *Atmos. Chem. Phys*., 9, 5785-5812, https://doi.org/10.5194/acp-9-5785-2009.

Yokelson, R. J., Andreae, M. O., & Akagi, S. K. (2013) Pitfalls with the use of enhancement ratios or normalized excess mixing ratios measured in plumes to characterize pollution sources and aging, *Atmos. Meas. Tech*., 6, 2155-2158, doi:10.5194/amt-6-2155-2013.

Zhou, S., Collier, S., Jaffe, D. A., Briggs, N. L., Hee, J., Sedlacek III, A. J., et al. (2017), Regional influence of wildfires on aerosol chemistry in the western US and insights into atmospheric aging of biomass burning organic aerosol, *Atmos. Chem. Phys*., 17, 2477-2493, doi:10.5194/acp-17-2477-2017.

Journal of Geophysical Research: Atmospheres

Supporting Information for

Aerosol mass and optical properties, smoke influence on O_3, and high NO_3 production rates in a western US city impacted by wildfires

Vanessa Selimovic[1], Robert J. Yokelson[1], Gavin R. McMeeking[2], Sarah Coefield[3]

[1]Department of Chemistry, University of Montana, Missoula, 59812, USA
[2]Handix Scientific LLC, 5485 Conestoga Court, Suite 104B, Boulder, CO, 80301, USA
[3]Missoula City-County Health Department, Missoula, MT 59801, USA

Contents of this file

Figures S1 to S10

Introduction

The supporting information contains:

- Ten figures: (S1—S5) High-resolution and hourly time series of species measured for each individual smoke event contributing to the analysis; (S6) Plot of the BC/PM ratio; (S7) Plot of MSC at 401 nm; (S8) Plot of MAC at 401 nm; (S9) Plot of MSC at 870 nm; (S10): Plot of MAC at 870 nm.

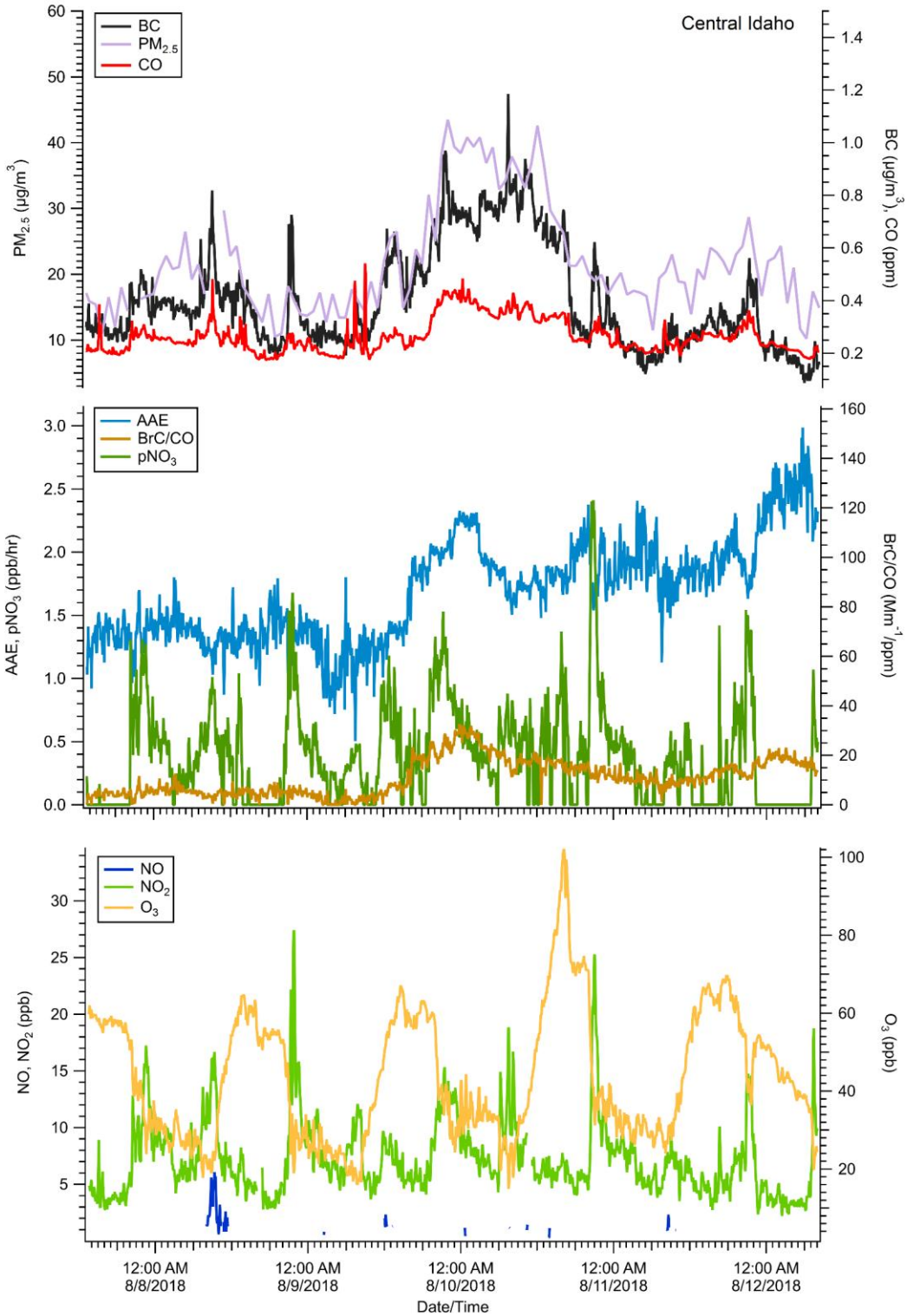

Figure S1. Time series of hourly $PM_{2.5}$, 5-minute BC, CO, NO_x, and O_3 measurements from Missoula. Hourly derived AAE and calculated p(NO_3) using 5-minute measurements of NO_2 and O_3 are also shown. Graph label (Central Idaho) represents our best guess at smoke source location based on satellite observations and back trajectory calculations.

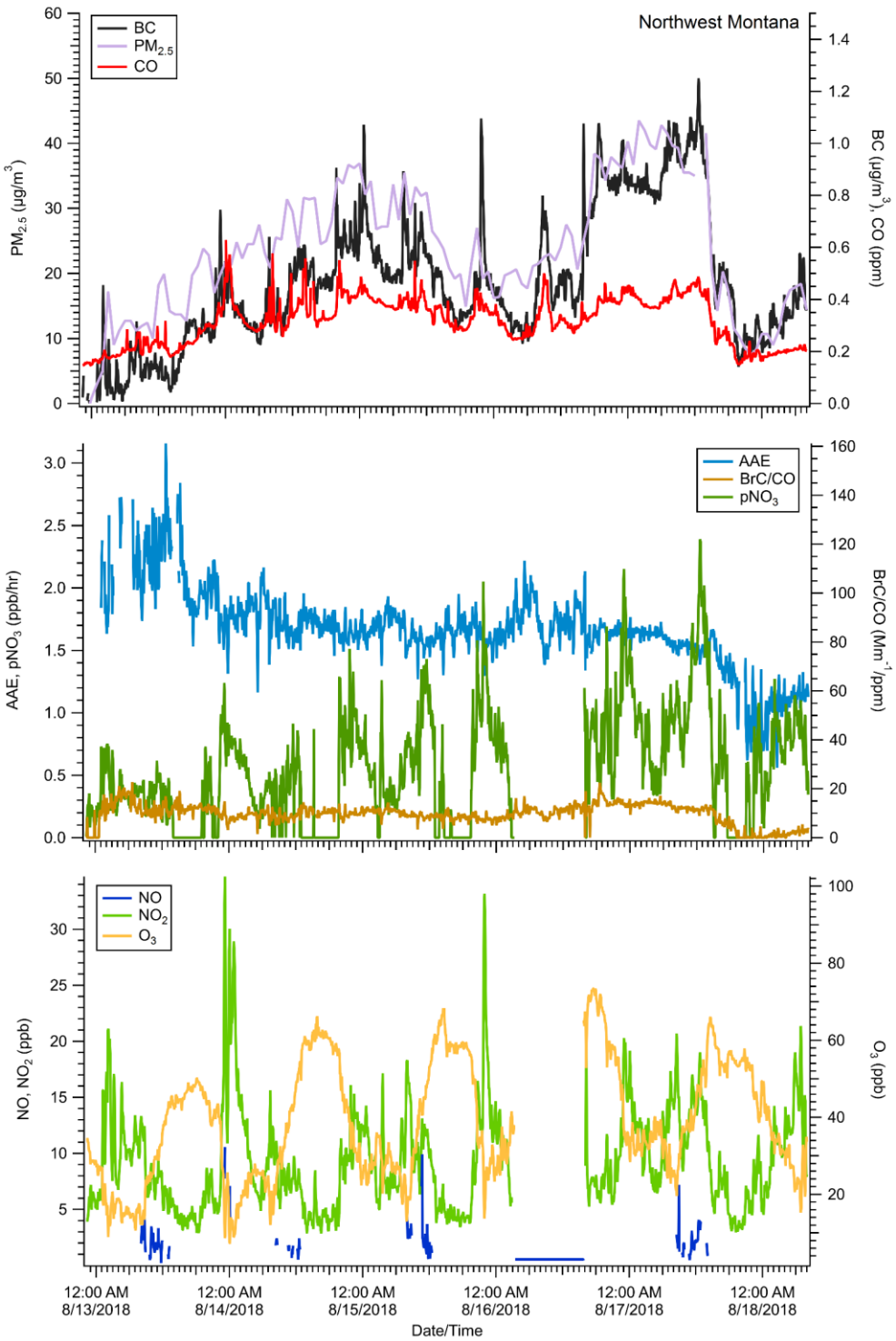

Figure S2. Time series of hourly $PM_{2.5}$, 5-minute BC, CO, NO_x, and O_3 measurements from Missoula. Hourly derived AAE and calculated $p(NO_3)$ using 5-minute measurements of NO_2 and O_3 are also shown. Graph label (Northwest Montana) represents our best guess at smoke source location based on satellite observations and back trajectory calculations.

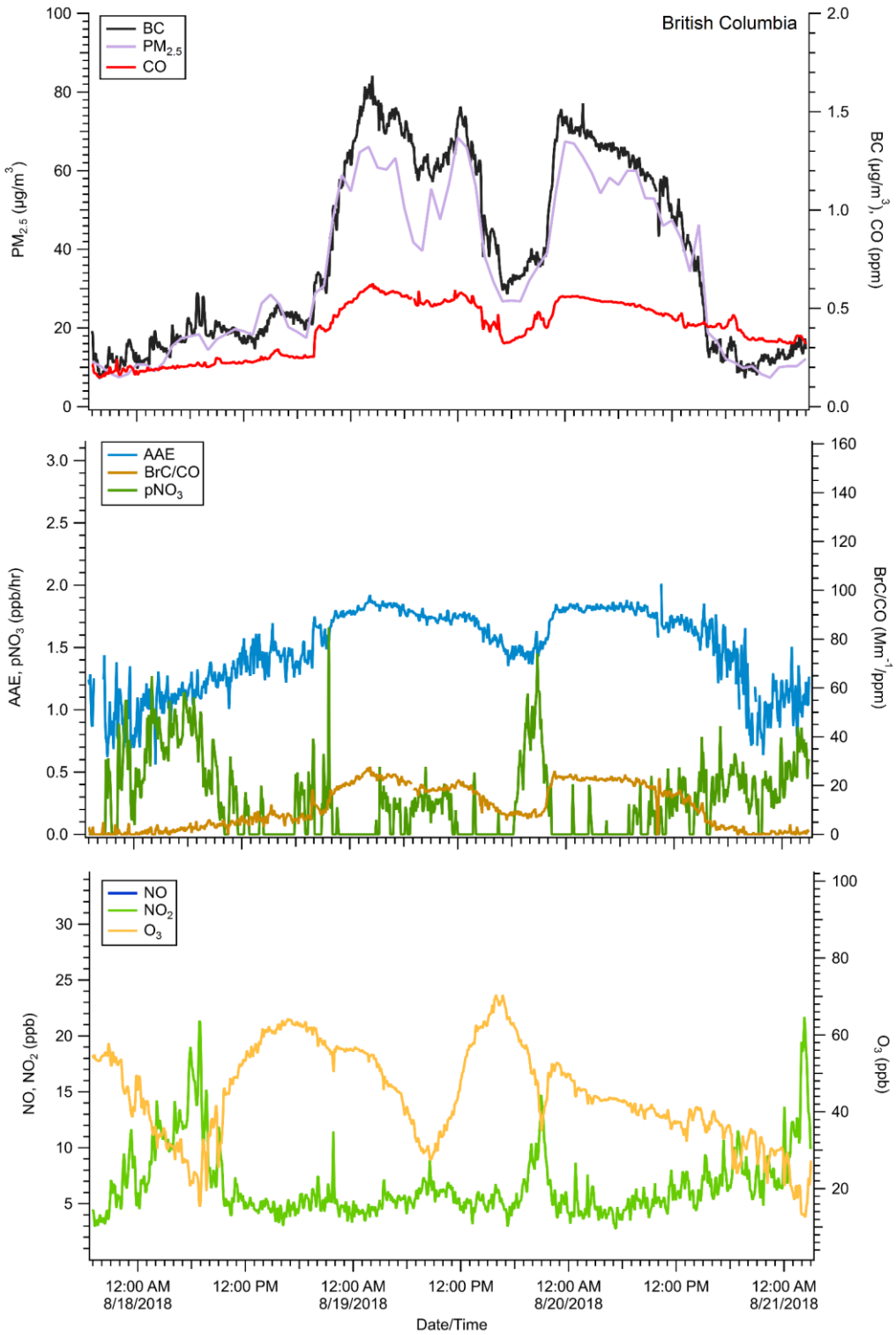

Figure S3. Time series of hourly $PM_{2.5}$, 5-minute BC, CO, NO_x, and O_3 measurements from Missoula. Hourly derived AAE and calculated $p(NO_3)$ using 5-minute measurements of NO_2 and O_3 are also shown. Graph label (British Columbia) represents our best guess at smoke source location based on satellite observations and back trajectory calculations.

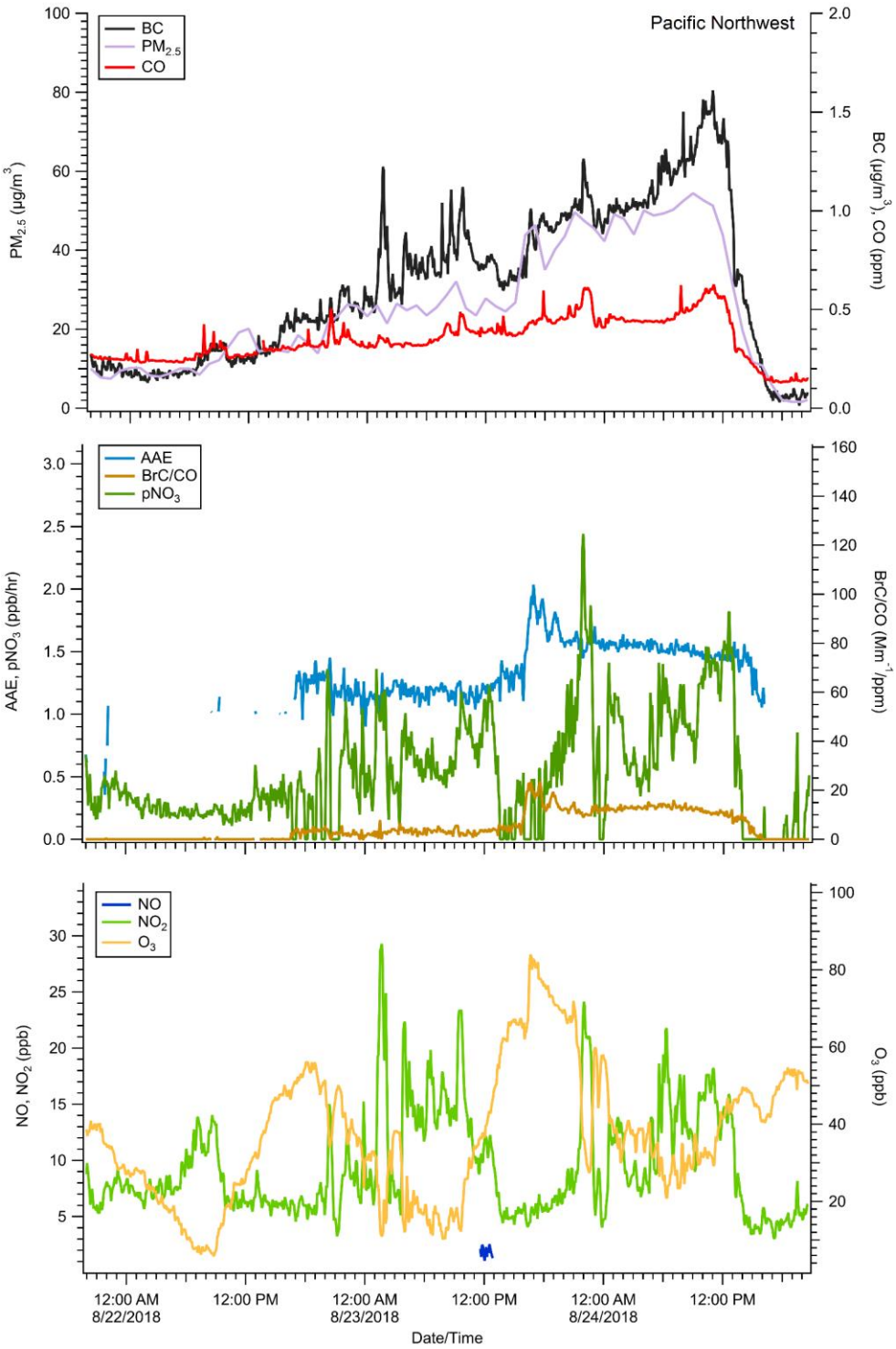

Figure S4. Time series of hourly $PM_{2.5}$, 5-minute BC, CO, NO_x, and O_3 measurements from Missoula. Hourly derived AAE and calculated p(NO_3) using 5-minute measurements of NO_2 and O_3 are also shown. Graph label (Pacific Northwest) represents our best guess at smoke source location based on satellite observations and back trajectory calculations.

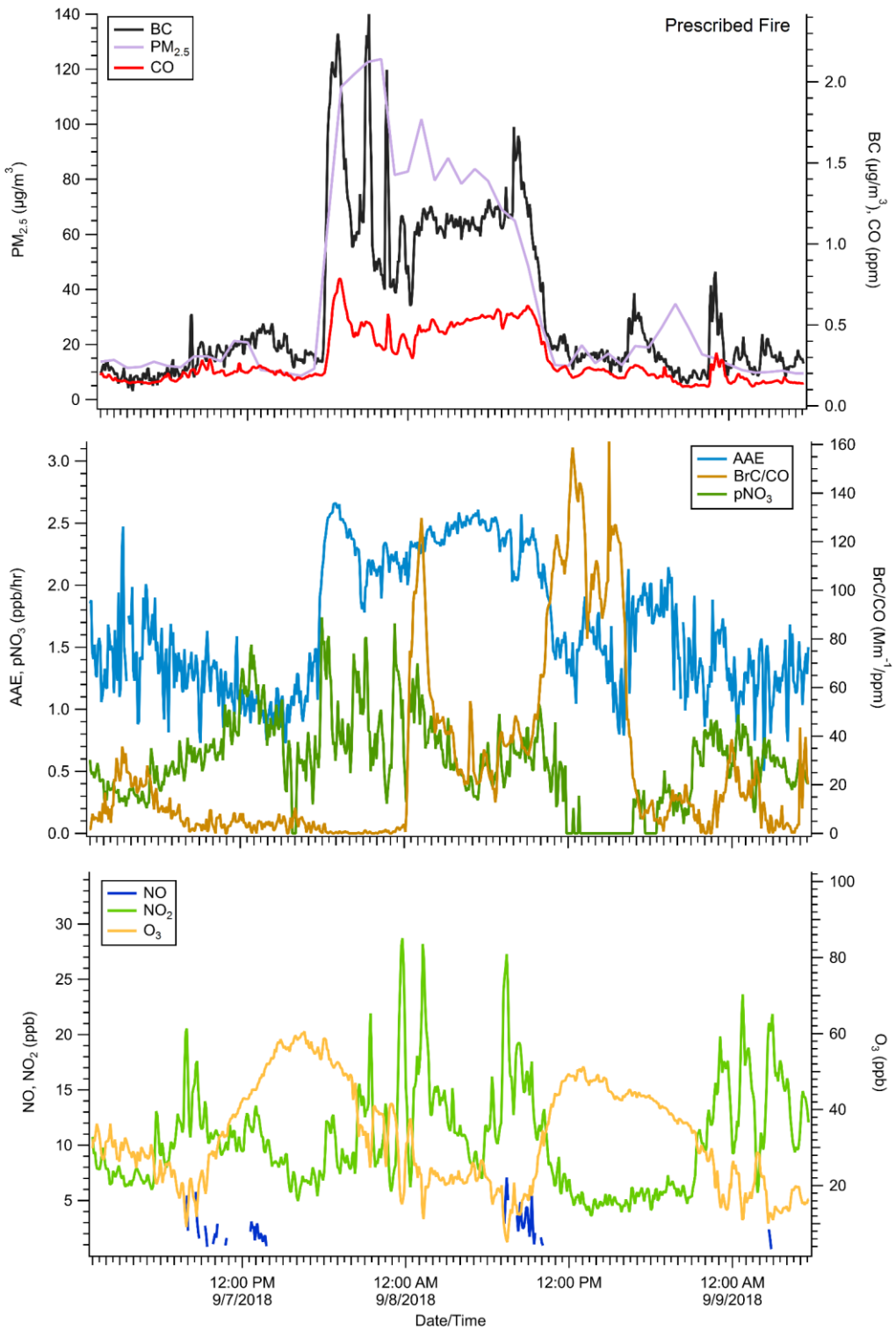

Figure S5. Time series of hourly $PM_{2.5}$, 5-minute BC, CO, NO_x, and O_3 measurements from Missoula for the one prescribed fire measured. Hourly derived AAE and calculated $p(NO_3)$ using 5-minute measurements of NO_2 and O_3 are also shown.

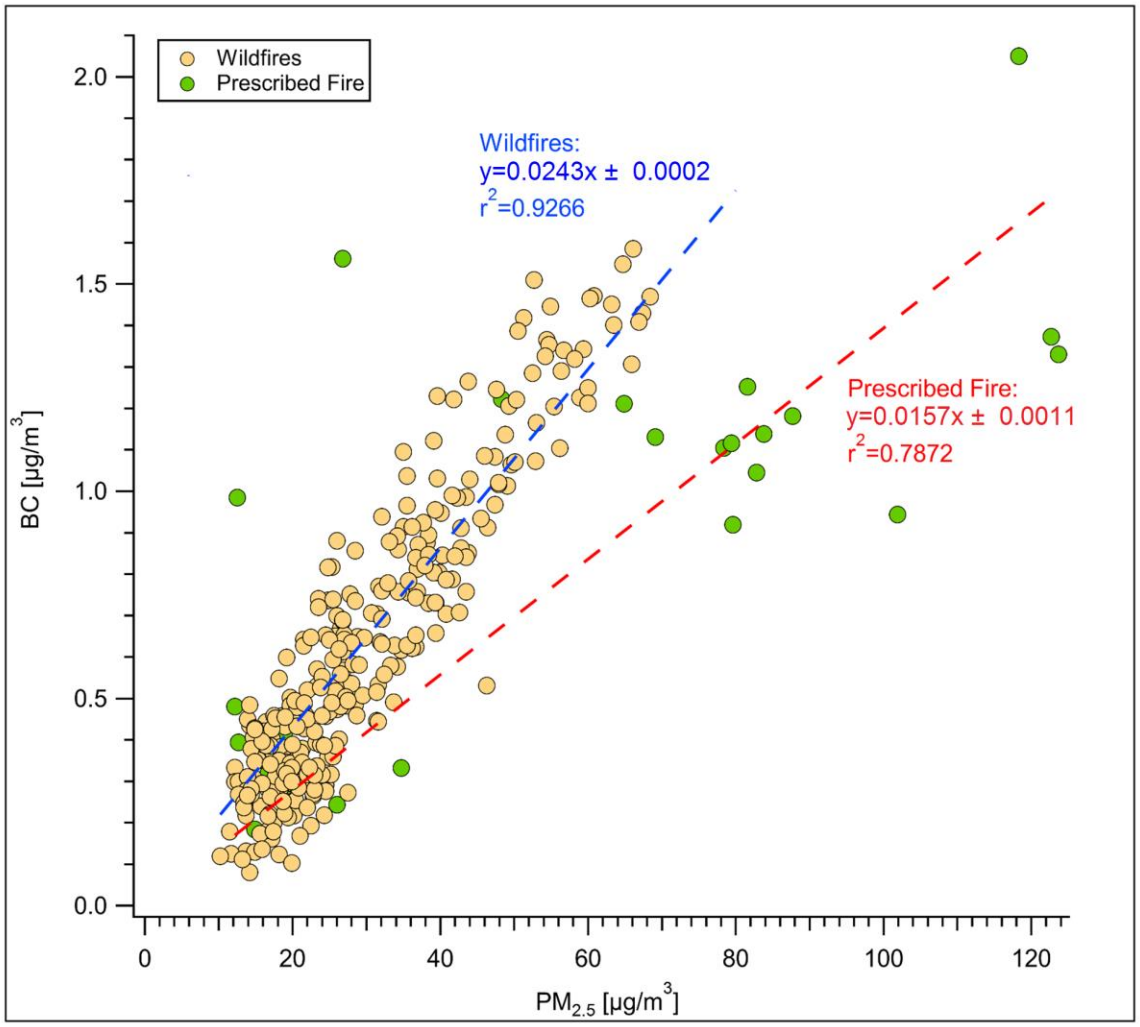

Figure S6. Hourly BC versus hourly $PM_{2.5}$. Slopes represent the corresponding BC/PM ratio.

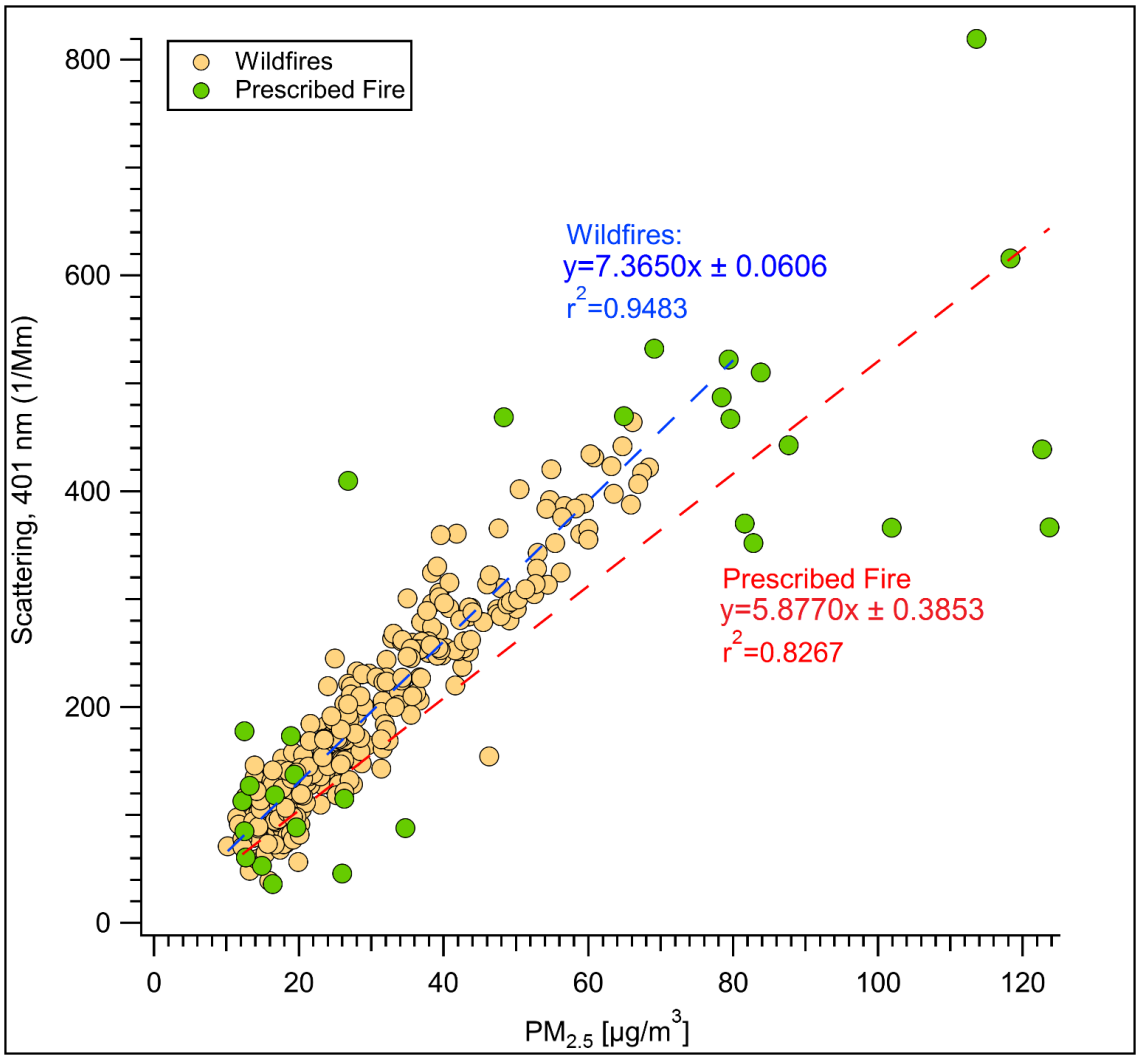

Figure S7. Hourly scattering measured by the PAX-401 versus hourly PM2.5. Slope values represent the corresponding mass scattering coefficients.

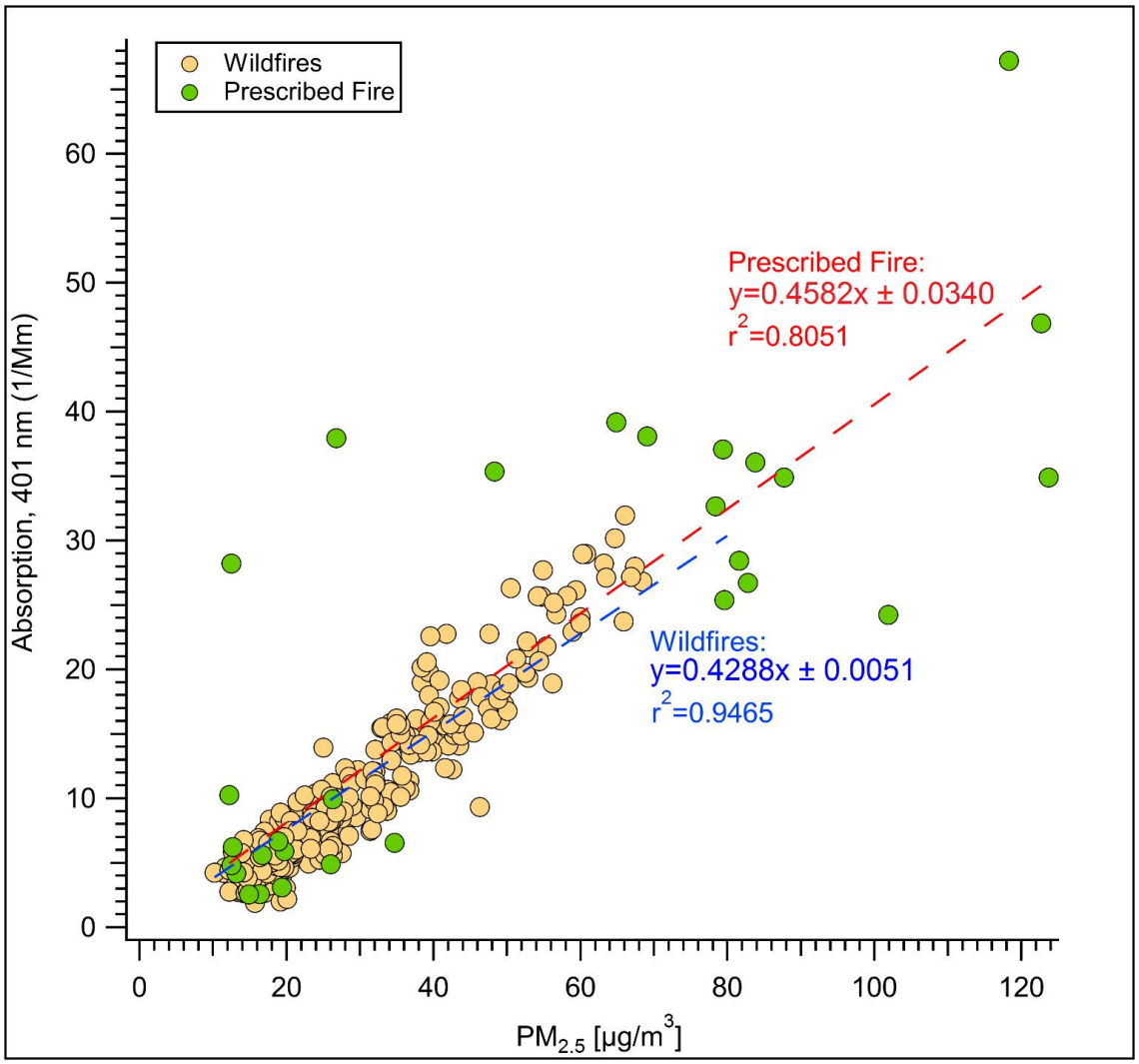

Figure S8. Hourly absorption measured by the PAX-401 versus hourly PM2.5. Slope values represent the corresponding mass absorption coefficients.

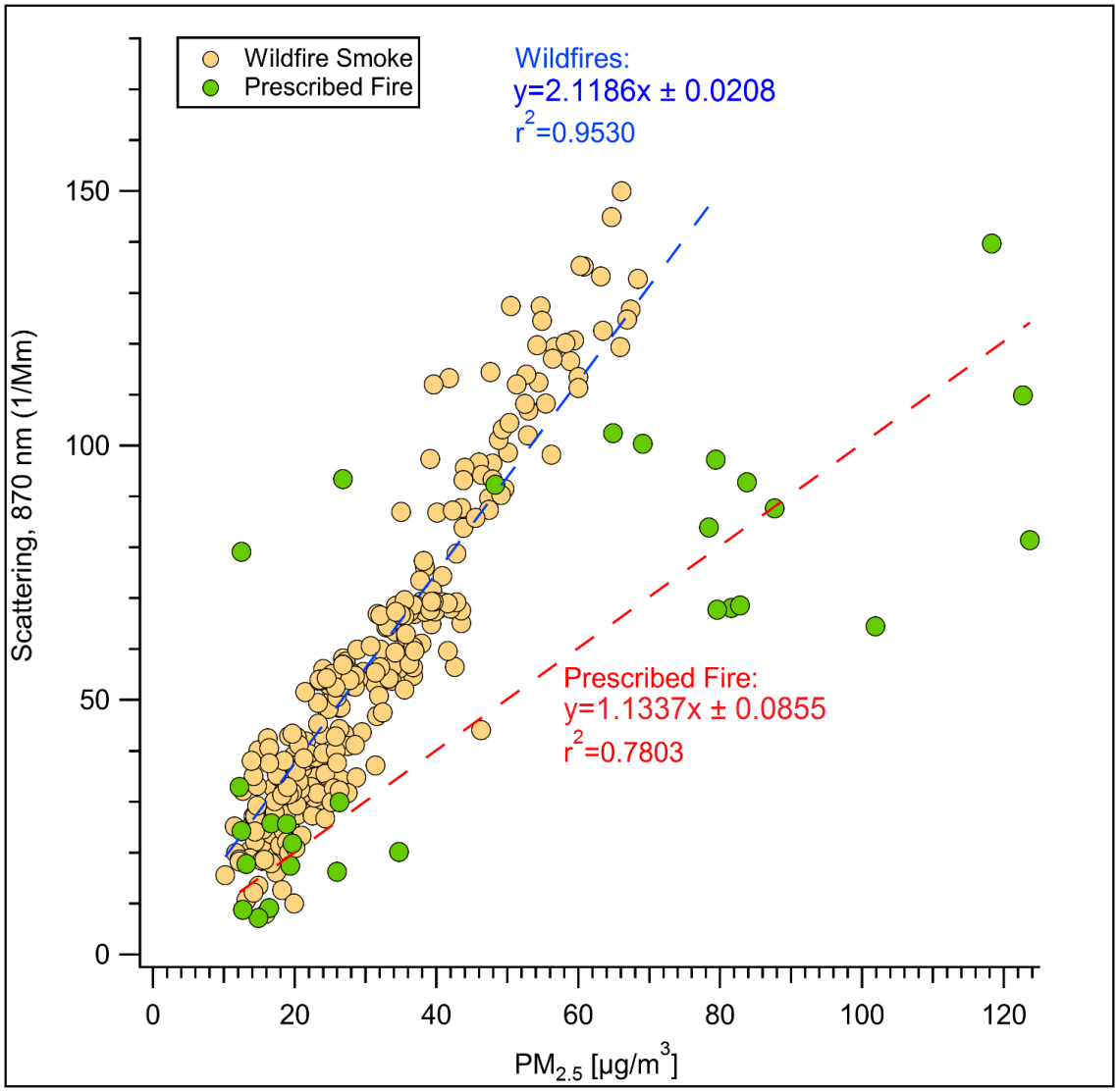

Figure S9. Hourly scattering measured by the PAX-870 versus hourly PM2.5. Slope values represent the corresponding mass scattering coefficients.

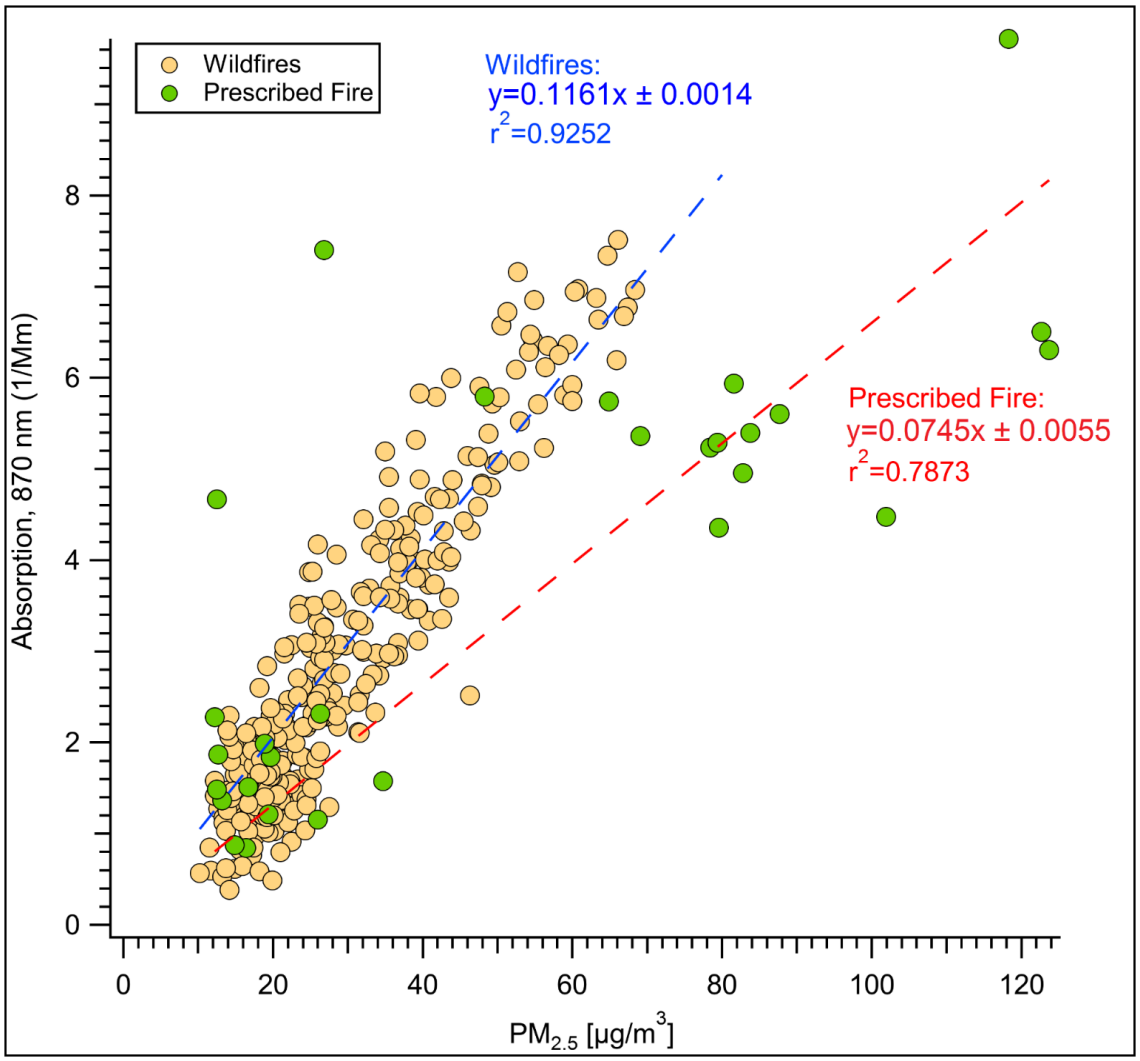

Figure S10. Hourly absorption measured by the PAX-870 versus hourly PM2.5. Slope values represent the corresponding mass absorption coefficients.